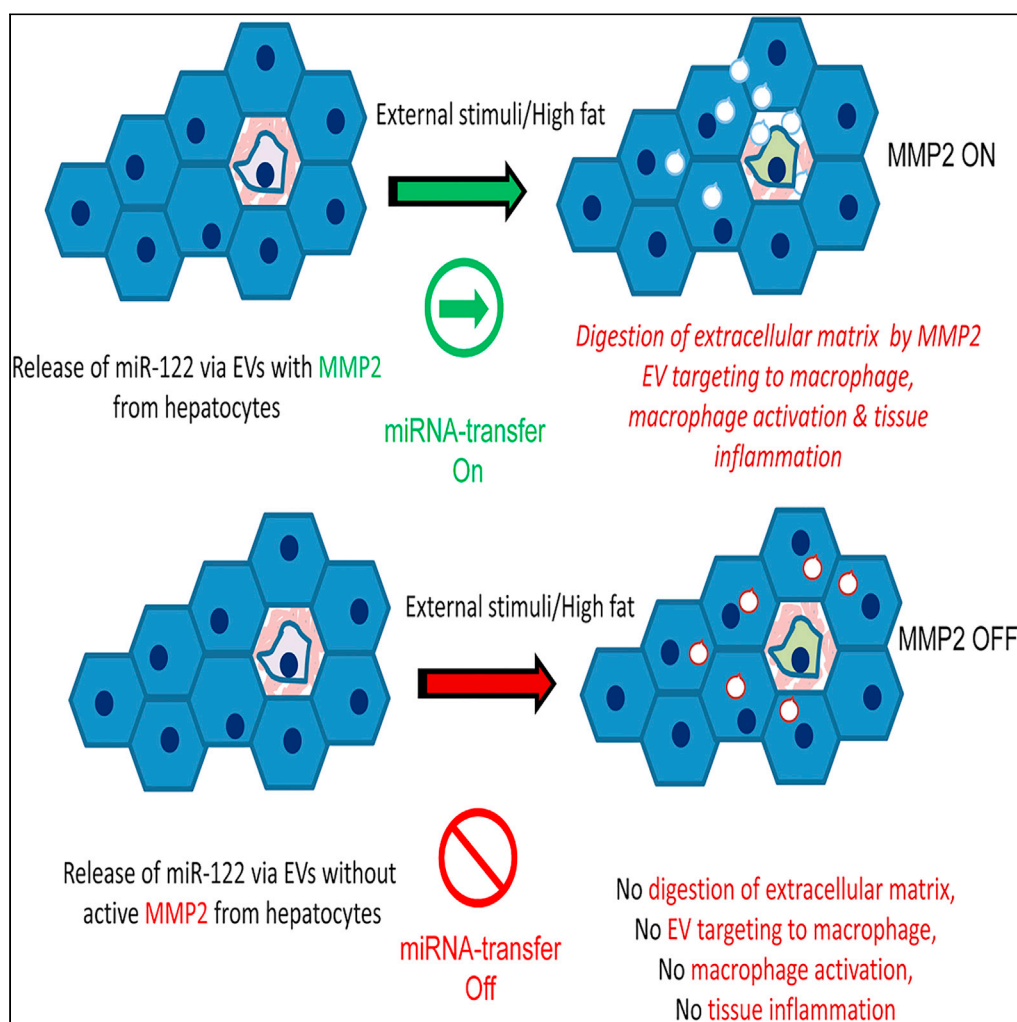


## Article

## Inhibition of extracellular vesicle-associated MMP2 abrogates intercellular hepatic miR-122 transfer to liver macrophages and curtails inflammation



Arnab Das,  
Sudarshana Basu,  
Diptankar  
Bandyopadhyay,  
..., Snehasikta  
Swarnakar, Partha  
Chakrabarti,  
Suvendra N.  
Bhattacharyya

suvendra@iicb.res.in

## Highlights

Hepatocytes on exposure to high lipid export proinflammatory miR-122 in mouse liver

Uptake of extracellular miR-122 induces inflammatory signals in liver macrophages

MMP2 on extracellular vesicles is essential for intercellular transfer of miRNA

Inhibition of MMP2 prevents miR-122 transfer and stops activation of macrophages

Das et al., iScience 24, 103428  
December 17, 2021 © 2021  
The Author(s).  
<https://doi.org/10.1016/j.isci.2021.103428>

## Article

## Inhibition of extracellular vesicle-associated MMP2 abrogates intercellular hepatic miR-122 transfer to liver macrophages and curtails inflammation

Arnab Das,<sup>1,7</sup> Sudarshana Basu,<sup>1,6,7</sup> Diptankar Bandyopadhyay,<sup>1,7</sup> Kamalika Mukherjee,<sup>1</sup> Debduiti Datta,<sup>1</sup> Sreemoyee Chakraborty,<sup>1,4</sup> Sayantan Jana,<sup>2</sup> Moumita Adak,<sup>3</sup> Sarpita Bose,<sup>5</sup> Saikat Chakrabarti,<sup>5</sup> Snehasikta Swarnakar,<sup>2</sup> Partha Chakrabarti,<sup>3</sup> and Suvendra N. Bhattacharyya<sup>1,4,8,\*</sup>

## SUMMARY

**Hepatic miRNA, miR-122, plays an important role in controlling metabolic homeostasis in mammalian liver. Intercellular transfer of miR-122 was found to play a role in controlling tissue inflammation. miR-122, as part of extracellular vesicles released by lipid-exposed hepatic cells, are taken up by tissue macrophages to activate them and produce inflammatory cytokines. Matrix metalloprotease 2 or MMP2 was found to be essential for transfer of extracellular vesicles and their miRNA content from hepatic to non-hepatic cells. MMP2 was found to increase the movement of the extracellular vesicles along the extracellular matrix to enhance their uptake in recipient cells. Inhibition of MMP2 restricts functional transfer of hepatic miRNAs across the hepatic and non-hepatic cell boundaries, and by targeting MMP2, we could reduce the innate immune response in mammalian liver by preventing intra-tissue miR-122 transfer. MMP2 thus could be a useful target to restrict high-fat-diet-induced obesity-related metaflammation.**

## INTRODUCTION

MicroRNAs (miRNAs) are 22-nucleotide-long regulatory RNAs that can repress protein synthesis from their target mRNAs by imperfect base pairing (Bartel, 2018; Filipowicz et al., 2008). Majority of mammalian genes are under miRNA regulation, and deregulation of miRNA activity and expression is associated with human diseases (Bartel, 2009). These tiny regulatory RNAs that primarily affect the post-transcriptional steps of gene expression can also be transferred across cell boundaries. Extracellular vesicle (EV) or exosome-mediated delivery of miRNA acts as a major way of exchanging genetic information between cells in mammalian tissues and organs (Valadi et al., 2007). The pathology of different diseases is found to be associated with deregulation of miRNA machineries including its export via EVs. Export of miRNAs via EVs not only plays a critical role in maintaining the homeostasis of gene expression in higher eukaryotes but also allows rapid response of donor cells under stress (Mukherjee et al., 2016).

Hepatic miRNA, miR-122, identified as a highly abundant liver-specific miRNA, has a significant role in controlling hepatic metabolic processes (Chang et al., 2004). Inhibition of miR-122 leads to downregulation of a number of lipogenic and cholesterol biosynthesis genes in the liver (Esau et al., 2006; Jopling, 2012). This in turn leads to reduced plasma cholesterol, increased hepatic fatty-acid oxidation, and reduced synthesis of hepatic lipids. Various studies on circulating miRNAs in patients with non-alcoholic fatty liver disease reveal a distinctive serum miRNA profile based on the progression of disease. Upregulated levels of miR-122, miR-192, and miR-375 could be correlated with disease severity in patients with non-alcoholic steatohepatitis (NASH) as compared with patients with steatosis only (Piroola et al., 2015).

The EVs are 30- to 100-nm-diameter particles, and presence of specific proteins and RNA cargo within the EVs make them unique and cell-type specific to deliver cargos to target cells where cell-type-specific uptake may occur either by receptor-mediated endocytosis or phagocytic activity of the recipient cells. EV-entrapped miRNAs are also secreted into the extracellular milieu (blood, serum, or plasma) and EV-associated circulating miRNAs, being identified as potential biomarkers for metabolic diseases, can act as paracrine and endocrine signals in circulation and can influence the target gene expression in recipient

<sup>1</sup>RNA Biology Research Laboratory, Molecular Genetics Division, CSIR-Indian Institute of Chemical Biology, 4 Raja S C Mullick Road, Kolkata 700032, India

<sup>2</sup>Infectious Diseases and Immunology Division, CSIR-Indian Institute of Chemical Biology, 4 Raja S C Mullick Road, Kolkata 700032, India

<sup>3</sup>Cell Biology and Physiology Division, CSIR-Indian Institute of Chemical Biology, 4 Raja S C Mullick Road, Kolkata 700032, India

<sup>4</sup>Academy of Scientific and Innovative Research, CSIR-Human Resource Development Centre, (CSIR-HRDC), Ghaziabad, India

<sup>5</sup>Structural Biology and Bioinformatics Division, CSIR-Indian Institute of Chemical Biology, 4 Raja S C Mullick Road, Kolkata 700032, India

<sup>6</sup>Present address: Department of Molecular Biology, Netaji Subhash Chandra Bose Cancer Research Institute, Kolkata, India

<sup>7</sup>These authors contributed equally

<sup>8</sup>Lead contact

\*Correspondence: suvendra@iicb.res.in

<https://doi.org/10.1016/j.isci.2021.103428>



cells (Basu and Bhattacharyya, 2014; Wang et al., 2019). Recently, a study has shown how, in alcohol-fed mice, miRNA-122 transferred via EVs to monocytes and liver Kupffer cells (KCs) sensitized them to LPS stimulation and pro-inflammatory cytokine production (Momen-Heravi et al., 2015).

How the EVs with their cargo get transferred through the extracellular matrix before they get delivered to recipient cells is an important question, and the matrix metalloproteases (MMPs) are interesting candidates to explore as players in EV transport (Shimoda and Khokha, 2017). Recently, MMP2 has been identified as a metalloprotease present in the EV released by osteoblast cells and was found to be essential for endothelial cell angiogenesis (Tang et al., 2019). MMP2 is recruited to the membranes via MMP14, which is known to act as an adapter protein of MMP2 for its association with biomembranes (Han et al., 2015). The mature form of MMP2 is an abundant MMP, and its level in the extracellular matrix is heavily regulated and found to be altered in the liver disease context (Wang et al., 2014). In different types of cancers, the importance of MMP2 is also well documented (Han et al., 2020).

In this article, we have detected MMP2 in EVs isolated from hepatic cells. The EV association of MMP2 is MMP14 dependent, and we have noted MMP2's functional role in cell-to-cell miRNA transfer. This process is blocked by the MMP2 inhibitor and restored by recombinant MMP2. The transfer of pro-inflammatory miR-122 from hepatocytes to liver resident macrophage cells is dependent on MMP2. We have also documented the retardation of movement of EVs in collagen matrix in the presence of MMP2 inhibitor. Thus, MMP2 can facilitate the functional miRNA cargo transfer across cell boundaries via EVs, and by blocking the EV transport with MMP2 inhibitor the expression of inflammatory cytokines can be perturbed in mammalian liver.

## RESULTS

### Detection of hepatic miR-122 in recruited monocytes and Kupffer cells in methionine choline-deficient diet-fed mice livers

Obesity is known to be accompanied by a low-grade, chronic inflammatory response orchestrated by pro-inflammatory cytokines like IL-1 $\beta$ , TNF- $\alpha$ , IL-6, and CCL2 (Berg and Scherer, 2005; Shoelson et al., 2006). The liver is also the site for inflammation in the obese state (Cai et al., 2005). Macrophages are known to play a significant role in hepatic inflammation and subsequent development of insulin resistance (Alisi et al., 2017). The hepatic macrophage population is heterogeneous and is composed of resident Kupffer cells (KCs) and infiltrating macrophages (recruited hepatic macrophages, RHMs). We wanted to explore the importance of liver-specific miRNAs in the activation of tissue macrophages on exposure to methionine choline-deficient (MCD) diet. To address this point, we chose to study a mice model of NASH by feeding the mice with MCD diet for 30 days (Caballero et al., 2010) and sorting the two macrophage populations using fluorescence-activated cell sorting (FACS) by differentially labeling them with fluorescent markers (Figure 1A). MCD diet-fed mice livers showed increased fat accumulation and hepatocyte ballooning characteristic of NASH (Figure 1B). Normal chow (Ch)-fed mice livers show none of these characteristics of NASH. Non-parenchymal cells were isolated from hepatic cell suspensions prepared from both MCD and Chow diet-fed mice livers followed by FACS sorting of F4/80<sup>+</sup>/CD11b<sup>+</sup> dual marker-positive KCs (R5) and F4/80<sup>low</sup>/CD11b<sup>+</sup> RHM cells that have low expression of F4/80 (R4) (Figure 1A) (Morinaga et al., 2015). The F4/80<sup>low</sup>/CD11b<sup>+</sup> set (R4) was sorted out as this represents fresh RHMs derived from circulating monocytes (Morinaga et al., 2015). The CD11b<sup>+</sup> population in MCD diet-fed mice livers appeared as two discrete fractions, the F4/80<sup>low</sup>/CD11b<sup>+</sup> set (R4) and the F4/80<sup>high</sup>/CD11b<sup>+</sup> set (R8). R8 cells appeared to be negligible in amount in Chow diet-fed mice and probably represents matured differentiated monocyte-derived macrophages and were not included in the analysis (Morinaga et al., 2015). We restricted our investigations to the R4 population as they represent fresh RHMs and hence would be more representative of conditions leading to infiltration and inflammation (Morinaga et al., 2015).

RT-qPCR analysis of RNA from isolated RHM (R4- F4/80<sup>low</sup>/CD11b<sup>+</sup> set) showed higher levels of hepatic miR-122 in RHM of MCD diet-fed mice livers as compared with those isolated from Chow diet-fed mice (Figure 1C; upper panel). However, levels of miR-16, another hepatic miRNA known to be present in circulation (Tan et al., 2014), remained unchanged (Figure 1C; lower panel). We also checked levels of precursor miR-122 in RHM to verify that miR-122 was not being endogenously induced to be expressed in the sorted RHM cells and was neither contributed by contamination from miR-122 expressing hepatic cells (Figure 1C; middle panel). Equivalent results were obtained for KC (R5- F4/80<sup>+</sup>/CD11b<sup>+</sup>) cells sorted from Chow and MCD diet-fed mice livers. KCs from MCD diet-fed mice show significantly elevated levels of hepatic miR-122

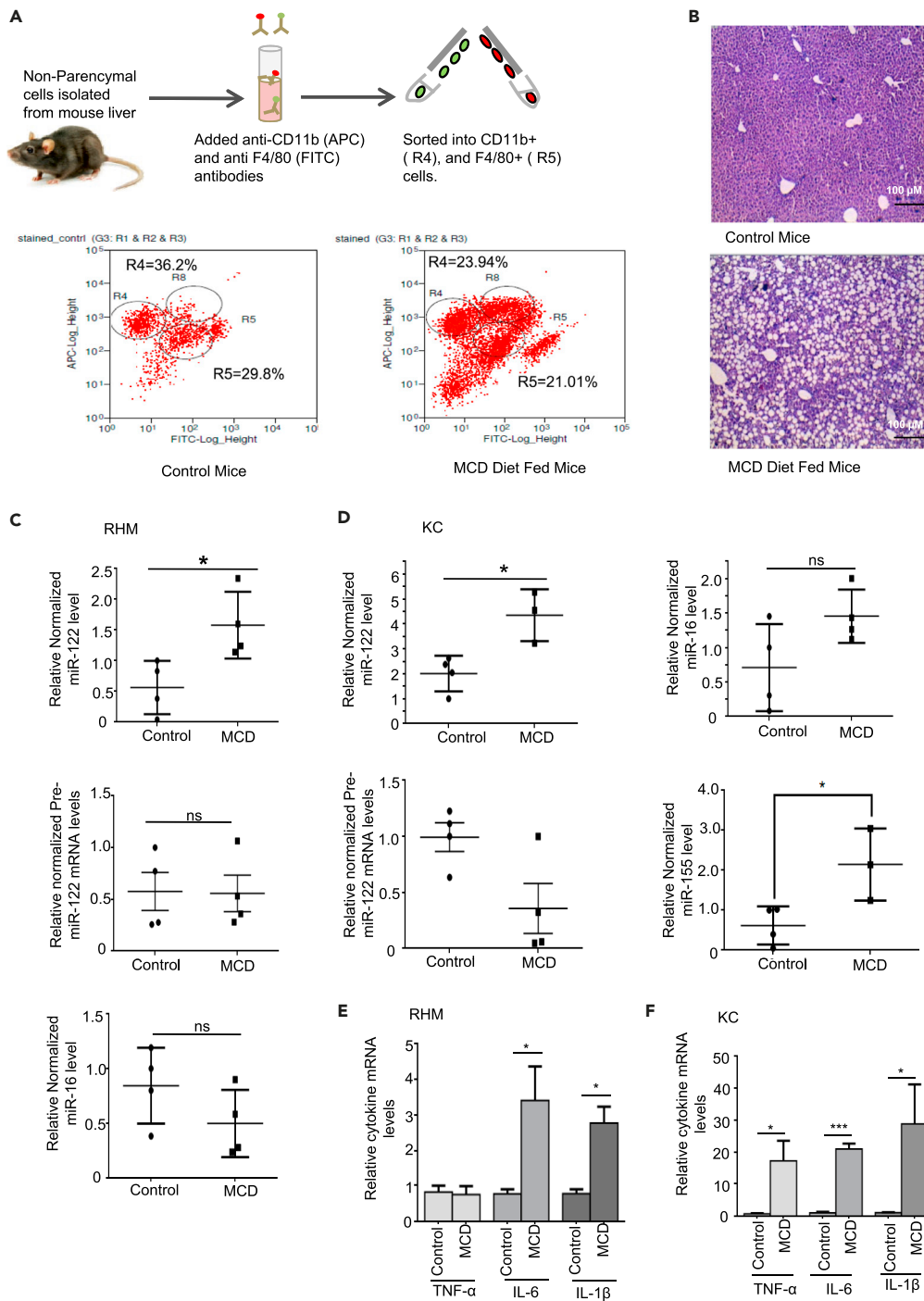


**Figure 1. Transfer of miR-122 from hepatic cells to tissue macrophages in MCD diet-fed mouse liver**

(A) Isolation and characterization of non-parenchymal cells (NPCs) from chow diet and MCD diet-fed mouse liver. Schematic diagram showing isolation and FACS sorting of NPCs from chow diet-fed (Control) versus MCD diet-fed mice livers with CD11b (APC) and F4/80 (FITC) gating.

(B) Hematoxylin and eosin-stained micrographs of control and MCD diet-fed mice liver sections. The scale bar depicts length equivalent to 100  $\mu$ m.

(C and D) Hepatic immune cells in MCD diet-fed mice show significantly higher levels of internalized miR-122 with respect to control. Relative internalized miR-122 level in sorted RHM cells (R4- F4/80<sup>low</sup>/CD11b<sup>+</sup> set) is shown (C, top panel). As a control, levels of pre-miR-122 (C, middle panel) and internalized miR-16 (C, bottom panel) have also been measured.

**Figure 1. Continued**

Relative levels of internalized miR-122 in sorted KCs (R5- F4/80<sup>+</sup>/CD11b<sup>+</sup>) is shown (D, top panel, left side). As a control, relative pre-miR-122 (D, bottom panel, left side) and internalized miR-16 (D, top panel, right side) and miR-155 levels (D, bottom panel, right side) have also been shown in the sorted KCs. miR-155 induction is characteristic of inflammatory response. The Ct values for pre-miR-122 were between 34 and 36 in all detections.

(E and F) Higher levels of internalized miR-122 correlates with increased expression of various pro-inflammatory cytokine mRNAs. Levels of pro-inflammatory cytokines (TNF- $\alpha$ , IL-6, and IL1 $\beta$ ) in sorted RHM cells (E) and KCs (F) from control and MCD diet-fed mice livers are shown. All mRNA and miRNA detections were done by RT-qPCR. RT-qPCR detection of cytokine mRNAs and pre-miR-122 was done using specific primers from 200 ng of cellular RNA. RT-qPCR detection of internalized miRNAs and miR-155 was done from 25 ng of isolated cellular RNA. Normalization of miR-122, miR-155, and miR-16 was done against U6 snRNA. Normalization of precursor miR-122 and cytokine mRNAs was performed with respect to 18S rRNA levels. Data represent mean  $\pm$  SD. All images are representative of at least four independent mice from each group. For statistical significance, minimum three independent experiments were considered in each case unless otherwise mentioned and error bars are represented as mean  $\pm$  S.D. p Values were calculated by using Student's t test. ns: non-significant, \*p < 0.05, \*\*\*p < 0.0001.

(Figure 1D; upper left panel), whereas changes in miR-16 levels were found to be non-significant (Figure 1D; upper right panel). Sorted KCs also do not induce transcription of pre-miR-122 as verified by decreased levels of precursor miR-122 in MCD diet-fed mice as compared with Chow diet (Figure 1D, lower left panel). Interestingly, in the sorted KCs there was an upregulation of miR-155, an inflammatory miRNA (Figure 1D, lower right panel).

Relative quantification of pro-inflammatory cytokine mRNAs was compared between control (Chow diet-fed mice) and MCD diet-fed group. Internalization of miR-122 correlated with increased levels of IL-6 and IL-1 $\beta$  in RHM (F4/80<sup>low</sup>/CD11b<sup>+</sup>) from MCD diet-fed mice livers (Figure 1E). Similar increases in TNF- $\alpha$ , IL-6, and IL-1 $\beta$  levels were detected in KC (F4/80<sup>+</sup>/CD11b<sup>+</sup> cells) cells (Figure 1F). Thus, both tissue-resident KCs and recruited monocytes from circulation are in an inflammatory state in the obese liver where elevated presence of hepatic miR-122 was noted.

**Induction of inflammatory cytokines in tissue-resident macrophages is caused by miR-122**

How does the liver-derived miR-122 increase in tissue-resident macrophages? We wanted to investigate the role of lipid-exposed liver cell-derived EVs in the induction of inflammation of receiving macrophages. Huh7 is a human hepatoma cell known to express miR-122. These cells, when exposed to a cholesterol-lipid concentrate present in the culture medium for 4 h, were found to export miR-122. EVs isolated from Huh7 cells (Basu and Bhattacharyya, 2014) were examined for their miRNA content (Figure 2A and 2B). As expected, we detected increased levels of miR-122 there. Three other miRNAs, miR-16, miR-24, and miR-21, also showed increased levels in EVs isolated from cholesterol-treated cells. miR-16 does show a relatively lower change in its level in released EVs after cholesterol exposure (Figure 2B). We have confirmed the luminal presence of EV-associated miR-122 in an RNase protection assay where the EV-associated miR-122 remains largely protected from RNases unless the EVs were treated with the detergent Triton X-100 to disrupt the membranous structure (Figure S2A). The functionality of the EV-derived miR-122 in recipient cells has been confirmed before (Ghoshal et al., 2021), and we have reconfirmed the repression of miR-122 targets in recipient cells treated with miR-122-containing EVs in subsequent assay using RAW264.7 cells as the recipient cells (Figure S2B). To test whether EVs isolated from lipid-treated hepatic cells could increase the inflammatory response in recipient macrophage cells, we added isolated EVs to various macrophages corresponding in origin to the donor hepatocyte (Figure 2A). We treated phorbol 12-myristate-13-acetate (PMA)-differentiated U-937 macrophages with EVs isolated from cholesterol-lipid concentrate-treated Huh7 cell. There, similar to what was noted in murine liver, addition of lipid-induced hepatocyte-derived EVs elevated pro-inflammatory cytokine mRNA levels in human macrophage cells (Figure 2C).

To determine the contribution of hepatic cell-derived EVs in the induction of the inflammatory phenotype, mouse primary hepatocyte cells were first treated with cholesterol-lipid concentrate for 4 h. EVs from the cell culture supernatant were then added to murine primary macrophages (KCs). Increased mRNA levels of the pro-inflammatory cytokines TNF- $\alpha$ , IL-6, and IL-1 $\beta$  were observed in recipient primary macrophage cells upon treatment with EVs derived from lipid-treated primary hepatocytes (Figure 2D). RT-qPCR assays detected increased levels of internalized miR-122 in the recipient macrophage cells as compared with the control (Figure 2E, left panel). However, levels of internalized miR-16, another miRNA known to increase in circulation in high-lipid condition (Tan et al., 2014), remained unaffected (Figure 2E, right panel). To

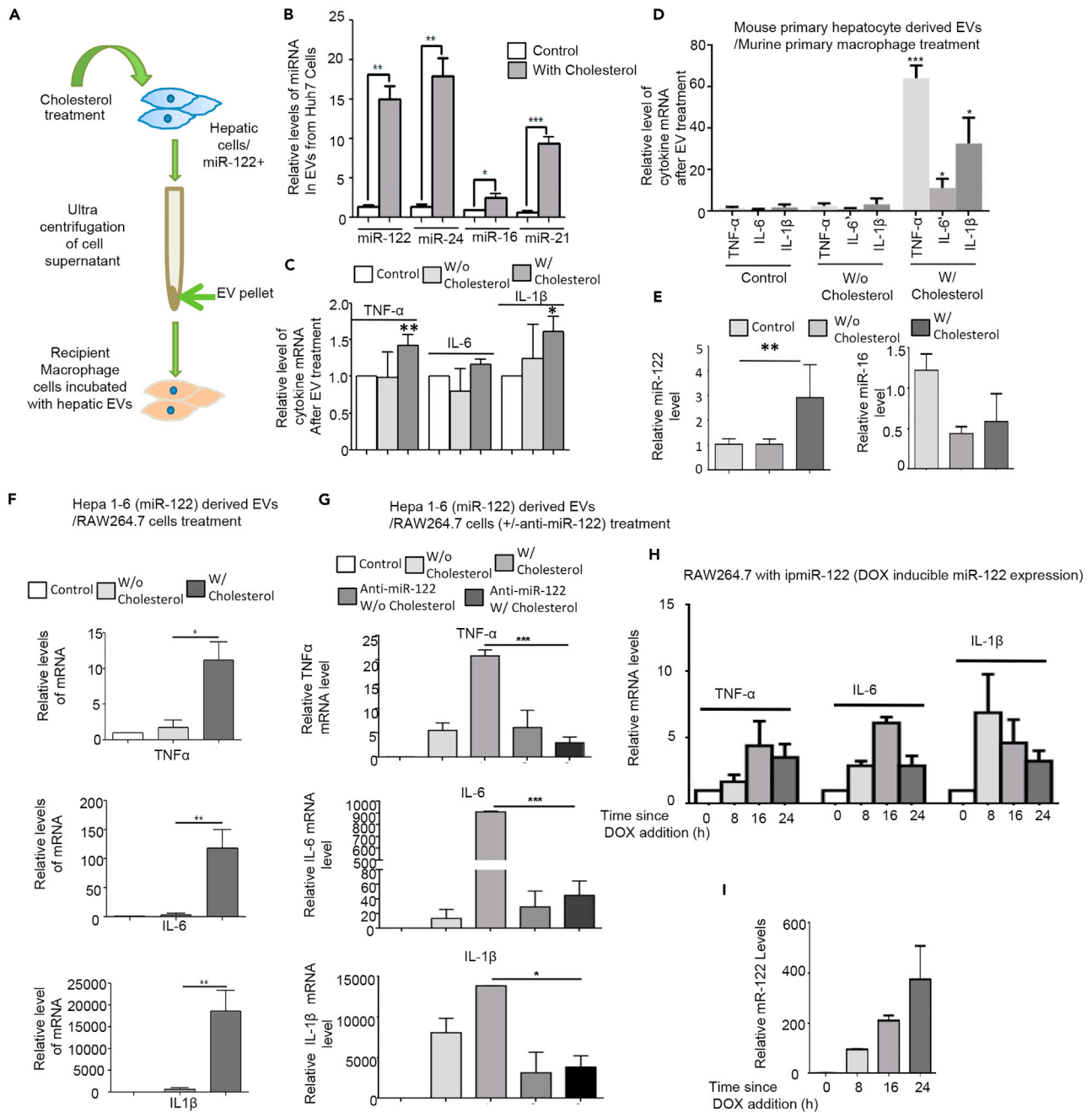


**Figure 2. Extracellular vesicle-mediated transfer of miR-122 from lipid-exposed hepatic cells to tissue macrophages activates them to express pro-inflammatory cytokines**

EV-associated miR-122 from lipid-treated hepatic cells when transferred to recipient macrophages induce higher levels of proinflammatory cytokine mRNAs. EVs were isolated from different types of hepatic cells treated with 5x cholesterol-lipid concentrate for 4 h. For the “w/o cholesterol” sets, equivalent volume of cholesterol-lipid concentrate was added to the cell supernatant after its collection from the cell culture plates. The “control” set represents immune cells to which no EVs were added. EV treatment was done for 16 h following which recipient cells were lysed and cellular RNA was isolated.

(A) Schematic diagram showing experimental procedure described above.

(B) Relative levels of EV-associated miRNAs secreted by Huh7 cells upon exposure to cholesterol-lipid concentrate.

(C) Relative levels of TNF- $\alpha$ , IL-6, and IL-1 $\beta$  in PMA-differentiated U937 cells to which EVs isolated from cholesterol-treated Huh7 cells were added.

(D) Relative proinflammatory cytokine mRNA levels in murine primary macrophages incubated with EVs isolated from cholesterol-treated primary hepatocytes.

(E) Internalized miR-122 (left panel) and miR-16 (right panel) in primary macrophages of experiment described in (D).

**Figure 2. Continued**

(F) Relative levels of TNF- $\alpha$  mRNA (top panel), IL-6 mRNA (middle panel), and IL-1 $\beta$  mRNA (bottom panel) in recipient RAW 264.7 monocytes incubated with EVs from cholesterol-treated Hepa1-6 cells expressing miR-122 (miR-122 expression-plasmid pmiR-122 transfected).

(G) Inhibition of internalized miR-122 in recipient macrophages leads to reversal of proinflammatory cytokine expression. EVs isolated from untreated (w/o cholesterol) and 5x cholesterol-lipid concentrate-treated (w/cholesterol) Hepa1-6 cells (pmiR-122 transfected) were added to RAW 264.7 cells prior transfected with anti-miR-122 oligos (Anti-miR-122 w/o cholesterol, anti-miR-122 w/ cholesterol). mRNA levels of TNF- $\alpha$  (top panel), IL-6 (middle panel), and IL-1 $\beta$  (bottom panel) were detected by RT-qPCR. See also [Figure S1](#).

(H and I) Presence of miR-122 in macrophage cells induces a pro-inflammatory phenotype. Induction of miR-122 expression in RAW264.7 leads to elevated levels of proinflammatory cytokine mRNAs. Tetracycline repressor-expressing RAW264.7 cells were transfected with inducible miR-122-expressing plasmids. Doxycycline, 400 ng/mL, was used to induce miR-122 expression. mRNA levels of TNF- $\alpha$ , IL-6, and IL-1 $\beta$  detected by RT-qPCR in cells harvested at indicated time points after Dox addition have been shown here (H). Relative miR-122 levels in RAW264.7 at various time points since DOX addition (I).

All mRNA and miRNA detections were done by RT-qPCR. RT-qPCR detection of cellular miRNAs was done from 25 ng of cellular RNA. RT-qPCR detection of EV miRNAs was done from 100 ng of isolated EV RNA. Normalization of miR-122 and miR-16 was done with respect to U6 snRNA. Normalization of precursor miR-122 and cytokine mRNAs was done with respect to 18S rRNA. Data represent mean  $\pm$  SD. (B-I) N = 3 replicates. p Values were calculated by using Student's t test. ns: non-significant, \*p < 0.05, \*\*p < 0.01, \*\*\*p < 0.0001.

See also [Figure S1](#).

determine the miR-122 dependence of this phenomenon, we isolated EVs from cholesterol-lipid-treated Hepa1-6 cells expressing miR-122 and added them to RAW 264.7 cells. Like in primary macrophage cells, RAW264.7 cells receiving the EVs from miR-122-transfected and cholesterol-treated Hepa1-6 cells also showed increased expression of pro-inflammatory cytokines ([Figure 2F](#)). In the subsequent experiment, to confirm the immunostimulatory role of miR-122 transferred from lipid-challenged hepatic cells, receiving RAW264.7 cells were transfected with anti-miR-122 oligos. Anti-miR-122-transfected cells showed marked decrease in various proinflammatory cytokine mRNAs like TNF- $\alpha$ , IL-1 $\beta$ , and IL-6 expression even after treatment with cholesterol-lipid-treated Hepa1-6 EVs ([Figure 2G](#)). These results strongly suggest the pro-inflammatory nature of the miR-122 exported from lipid-loaded hepatic cells. The extracellular miR-122, taken up by receiving macrophages, enhances the expression of proinflammatory cytokines and thereby ensures a more activated state of inflammation in the recipient cells.

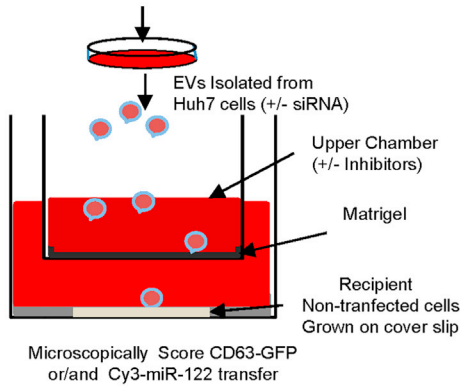
To make a strong correlation of EV-derived miR-122 and inflammatory response, we expressed miR-122 from a doxycycline (DOX)-inducible expression vector in naive RAW264.7 cells and checked cytokine mRNA levels over time when cells were incubated with DOX. The induction of miR-122 resulted in an accumulation of mature miR-122 over time upon induction with DOX. The increase in cellular miR-122 levels was found to correlate with the expression increase of cytokine mRNAs ([Figures 2H and 2I](#)). Interestingly, after a threshold of expression, happening at 24 h of miR-122 induction, effectiveness of miR-122 for cytokine induction gets impaired possibly due to jeopardized miRNP balance happening for other important miRNAs present there.

Do the EVs released by hepatic cells enter and affect the cytokine expression in tissue-resident macrophages? We isolated EVs packed with miR-122 from the culture supernatant of Hepa1-6 cells expressing miR-122. The EVs were injected into normal BALB/c mice (adult, 8–10 weeks) through tail vein, and hepatic non-parenchymal cells were isolated and analyzed for expression of different cytokines ([Figure S1A](#)). Compared with PBS-injected groups, mice injected with miR-122-containing EVs showed an increase in miR-122 levels in isolated hepatic non-parenchymal cells, along with an elevation in the expression of inflammatory cytokines ([Figures S1B–S1C](#)). The circulatory miR-122 level in miR-122 EV-injected mice also showed an elevation with no corresponding change in serum miR-16 level ([Figure S1D](#)). These data suggest miR-122-containing EV-dependent inflammatory response in murine liver.

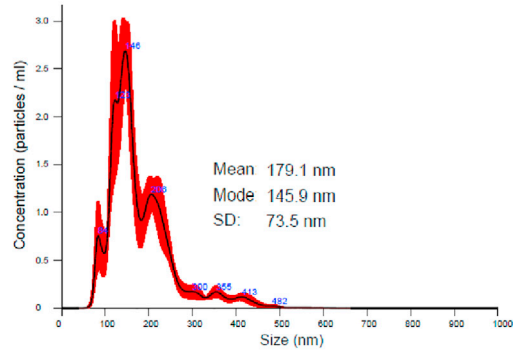
**Blocking of MMP2 affects miRNA cargo transfer between human cells**

How do EVs move within the matrix of a tissue? In the liver, the extracellular matrix is rigid and composed of high levels of collagen. We expect that the presence of specific proteases on the surface of EV may do the job of degrading the matrix and MMPs are the best candidate for doing that. We explored the effect of different inhibitors and factor-specific siRNAs against MMPs to score their effect on EV-mediated miRNA transfer in human cells in a microscopy-based assay. In this assay the recipient HeLa cells were grown on coverslip in a 24-well cell culture format with the insert. The insert separated the upper compartment that was used for layering of Matrigel. Isolated EVs from human hepatoma cell Huh7 transfected with Cy3-labeled miR-122 were used to study the transfer of Cy3-labeled miR-122 to recipient HeLa cells. The isolated EVs were added in the upper chamber, which separated the EVs from target cells present in the

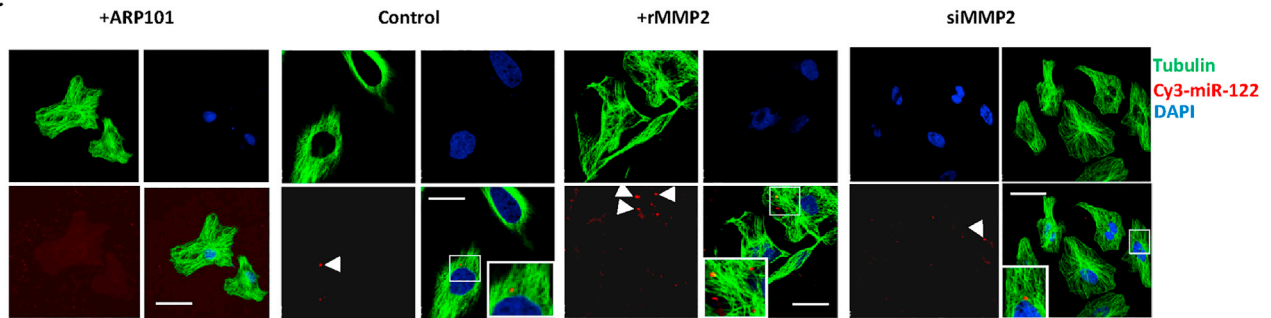
**A** CD63-GFP encoding plasmid  
or Cy3-miR-122 transfection



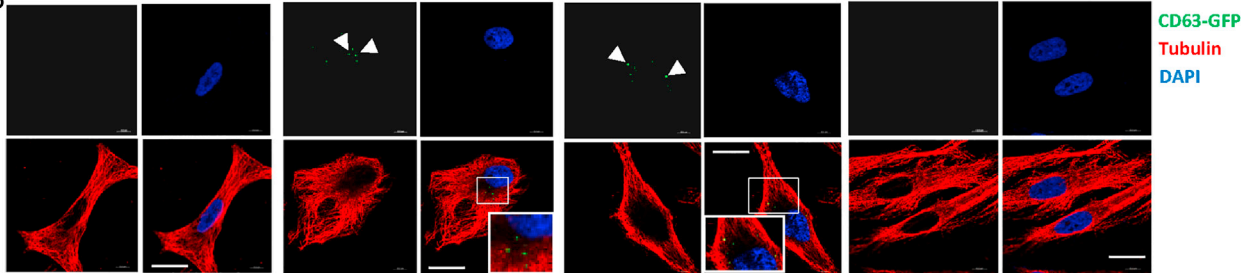
**B**



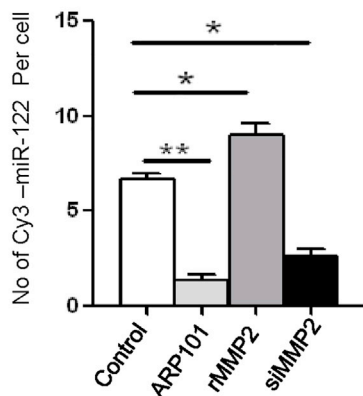
**C**



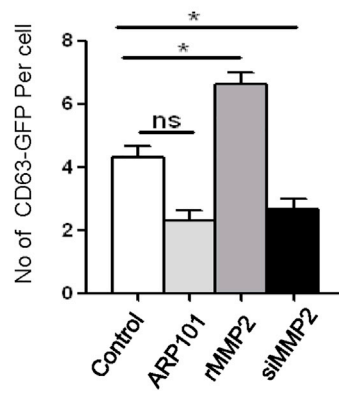
**D**



**E**



**F**



**G**

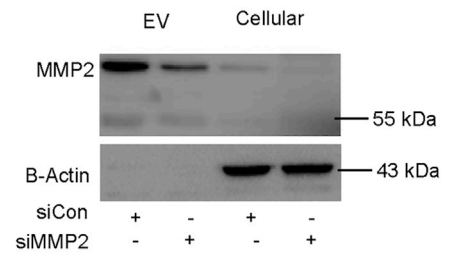


### Figure 3. MMP2-dependent entry of EV in recipient cells

(A–C) Experimental scheme is shown in (A) Donor Huh7 cells were transfected with Cy3-labeled miR-122 oligonucleotides and siMMP2 before the EVs were isolated. The quantity and size distribution of the EVs were characterized by nanoparticle tracking analysis (B). Recipient HeLa cells were seeded on the gelatin-coated coverslips at the lower chamber of the 24-well plates. The bottom of 0.4  $\mu\text{m}$  pore-containing inserts was coated with diluted growth factor reduced Matrigel (3 mg/ml) and incubated at 37°C for 30–45 min. After incubation, EVs were added into the inserts with the presence or absence of ARP101 or DMSO or rMMP2 and then they were kept for incubation for 24 h (A). On the next day, after cell fixation, permeabilization, and staining for  $\beta$ -tubulin, cells were imaged (C). Arrowheads indicate internalized Cy3-miR-122 signals in recipient HeLa cells. The scale bar depicts length equivalent to 10  $\mu\text{m}$  and inset zoomed 5 times.

(D) Donor Huh7 cells were transfected with CD63-GFP and siCon or siMMP2, followed by EV isolation and added into the inserts. The number of CD63-GFP transfer from donor cell EV to recipient HeLa cell was also quantified by counting green dots of CD63-GFP from three different sets, 5 fields/set, 5 cells/field. EVs from siCon-treated cells were used as control. ARP101 and rMMP2 were added along with EVs from CD63GFP-expressing cells in respective condition. Arrowheads show internalized CD63-GFP signals in recipient HeLa cells. The scale bar depicts length equivalent to 10  $\mu\text{m}$  and inset zoomed 5 times.

(E–G) miR-122 transfer from donor cell EV to recipient HeLa cell was quantified by counting red dots of Cy3-miR-122 from three different sets, 5 fields/set, 5 cells/field (E). CD63-GFP transfer from donor cell EVs to recipient HeLa cell was quantified by counting green dots of CD63-GFP from three different sets, 5 fields/set, 5 cells/field (F). The downregulation of MMP2 expression was observed when siMMP2 was transfected to donor cells by western blotting (G). For statistical significance, minimum three independent experiments were considered in each case unless otherwise mentioned and error bars are represented as mean  $\pm$  S.E.M. p Values were calculated by using Student's t test. ns: non-significant, \*p < 0.05, \*\*p < 0.01.

See also [Table S1](#).

lower chamber by a Matrigel layer. The transferred Cy3-labeled miRNAs were visualized by subjecting the recipient cell co-stained for tubulin to confocal microscopy imaging ([Figure 3A](#)). The inhibitors were applied in the upper chamber while siRNAs against specific proteins were co-transfected along with Cy3-miR-122 in donor Huh7 cells that were used for collecting EVs. The EVs used in the experiment were analyzed by Nanoparticle tracking analyzer ([Figure 3B](#)). We documented defective Cy3-miR-122 transfer happening to recipient cells treated with ARP101 as an inhibitor of MMP2 ([Jo et al., 2011](#)). Similar results were also observed with EVs isolated from MMP2-deficient Huh7 donor cells ([Figures 3C and 3E](#)). Interestingly, transfer of GFP-tagged CD63-positive EVs to recipient cells was also found to be impaired by ARP101 and siMMP2 when EVs were isolated from Huh7 cells expressing CD63-GFP ([Figures 3D and 3F](#)). siRNA-mediated knockdown of MMP2 was confirmed by western blot analysis of cellular and EV levels of MMP2 in siCon versus siMMP2-transfected donor Huh7 cells ([Figure 3G](#)).

### Functional transfer of miRNA from hepatic cells requires MMP2

What function does MMP2 have on EV-mediated cargo transfer between hepatic cells? To explore the exact role of MMP2 in miRNA transfer, we incubated miR-122-containing EVs derived either from naive or pmiR-122-transfected Huh7 cells with recipient HepG2 cells grown in Matrigel. We documented a transfer of miRNA into HepG2 cells that otherwise do not express miR-122. Furthermore, we noticed blocking of this transfer of miRNA when incubated with ARP101, the MMP2 inhibitor ([Figure 4A](#)). The transfer of mature miR-122 via EVs does not show any increase in the pre-miR-122 level in recipient HepG2 cells when compared with the control group ([Figure S2C](#)), which rules out the possible induction of miR-122 expression in recipient cells from the miR-122 expression plasmid that could have been transferred from Huh7 donor cells. Treatment of donor Huh7 cells with anti-miR-122 blocks the transfer of miR-122 to recipient cells ([Figure 4A](#)). A similar level of miR-122 transfer from donor HeLa cells, ectopically expressing miR-122, to HepG2 has been documented, and the MMP2 inhibitor blocked the transfer of miR-122 ([Figure 4B](#)). Does the transferred miRNA become functionally active in the recipient cells? We used miR-122 reporter mRNA to test the functional transfer of miR-122 in recipient cells. The transferred miR-122 could repress the RL-reporter having one perfect miR-122-binding site in HepG2 recipient cells, and a fold repression of the reporter has been scored against the RL reporter without miRNA-binding sites ([Figures 4C and 4D](#)) ([Basu and Bhattacharyya, 2014](#)). Inhibition of MMP2 by ARP101 reduced the miR-122 activity transfer to recipient HepG2 cells both from Huh7 and HeLa donor cells ([Figures 4E and 4F](#)). Interestingly, when EVs isolated from Huh7 cells expressing miR-122 were incubated with Huh7 cells we could see a drop in cellular miR-122 content. This may be explained by a reduced self-transfer of miR-122 to the donor cell that itself gets reduced in the presence of MMP2 inhibitor ARP101 ([Figure 4G](#)). The ARP101 itself, when applied to miR-122-expressing HepG2 cells, does not induce any change in miR-122 activity as fold repression of miR-122 target containing luciferase mRNA remains unaltered in ARP101-treated cells compared with DMSO-treated control ([Figure S2E](#)). Finally, the reduction in cellular mRNA levels of endogenous miR-122 targets, Aldolase A and CAT-1, in recipient RAW264.7 cells that were treated with pmiR-122-expressing Huh7 EVs, confirmed that the transferred miR-122 was indeed functionally active in the recipient cells ([Figure S2B](#)). The result described here point out to an important role of MMP2 in the transfer of functional cargo miRNA in mammalian cells and thus is an essential component of miRNA activity regulation in a tissue.

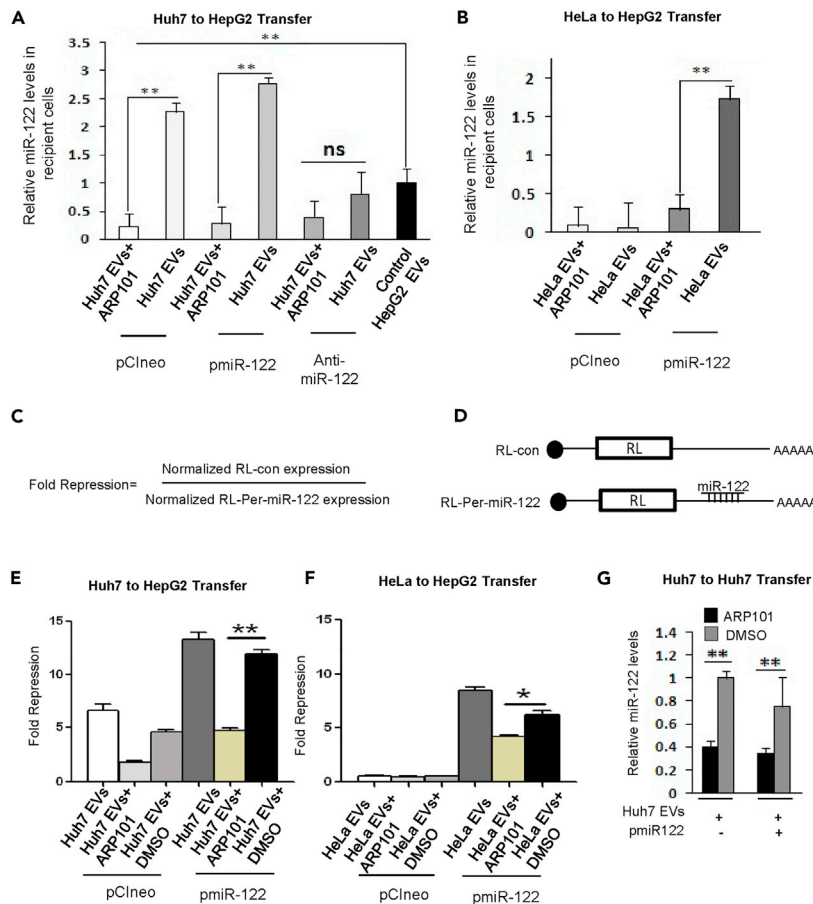


**Figure 4. Functional transfer of miR-122 between hepatic cells requires MMP2 activity**

(A and B) ARP101 inhibits the transfer of miR-122-containing EVs from donor cell to recipient cells. The transfer of EVs from hepatic cell lines was checked by using a specific MMP2 inhibitor ARP101 (12.5  $\mu\text{M}$ ). Huh7 (A) and HeLa (B) cells were chosen and transfected with miR-122-expressing pmiR-122 or anti-miR-122 oligos and EVs were isolated. HepG2 cells were taken as recipient cell. To check the transfer, transwell inserts (0.4  $\mu\text{m}$ , SPL) were taken and 100  $\mu\text{L}$  of 3 mg/ml diluted Matrigel was coated and solidified previously. In the lower chamber, HepG2 cells were seeded in complete DMEM with 10% fetal calf serum (FCS). EVs were added to the medium in the inserts and incubated for 30 min at 37°C. Serum-free DMEM was added onto the inserts with ARP101. In the control sets, the same amount of DMSO (v/v) was added. This was then incubated for 24 h. On the next day, RNA was isolated by using the Trizol RNA isolation method from HepG2 cells and cDNA was synthesized followed by real-time PCR for miR-122 by using miR-122 specific primers. Normalization was done with respect to U6 snRNA. Data represent mean  $\pm$  SD.

(C–F) Luciferase activity showed the repression of miR-122 reporter in recipient cells by transferred miR-122 from donor cells. The fold repression is the ratio of normalized expression levels obtained with RL-con and RL miR-122 reporter having one miR-122 perfect binding site (C and D). In similar experiments described in A and B, the repressive activities in the presence or absence of ARP101 were measured in HepG2 cells that do not express miR-122 otherwise. Huh7 and HeLa cells were overexpressed with miR-122, and EVs were isolated and added to the Matrigel-coated 0.4  $\mu\text{m}$  inserts. Recipient HepG2 cells, transfected either with pCIneo or pmiR-122 plasmid, were co-transfected with either RL-con or RL-per-miR-122 plasmids in parallel sets. To detect fold repression in HepG2,  $10^6$  cells in a 10-cm<sup>2</sup> well were transfected with 150 ng of each of the plasmids. Normalization was done with a Firefly (FF) luciferase construct, which was co-transfected along with the RL constructs (1  $\mu\text{g}$  for  $1 \times 10^6$  cells). After 24 h of transfection, cells were split and seeded in the lower chamber of the transwell insert. ARP101 was added. The whole set was incubated for 24 h again in presence of EVs from donor cells. Data represent mean  $\pm$  SD. N = 3 replicates.

(G) miR-122 expression was checked by ARP101 in donor cells. Huh7 cells were transfected with pmiR-122 and seeded in Matrigel with or without MMP2 inhibitor ARP101 in 24-well plates and incubated for 24 h. Cells were isolated from Matrigel and RNA was isolated followed by cDNA and real-time PCR for miR-122 and normalization of value obtained were done against U6 snRNA. Data represent mean  $\pm$  SD. N = 3 replicates. p values were calculated by using Student's t test. ns: non-significant, \*p < 0.05, \*\*p < 0.01.

See also Figure S2.

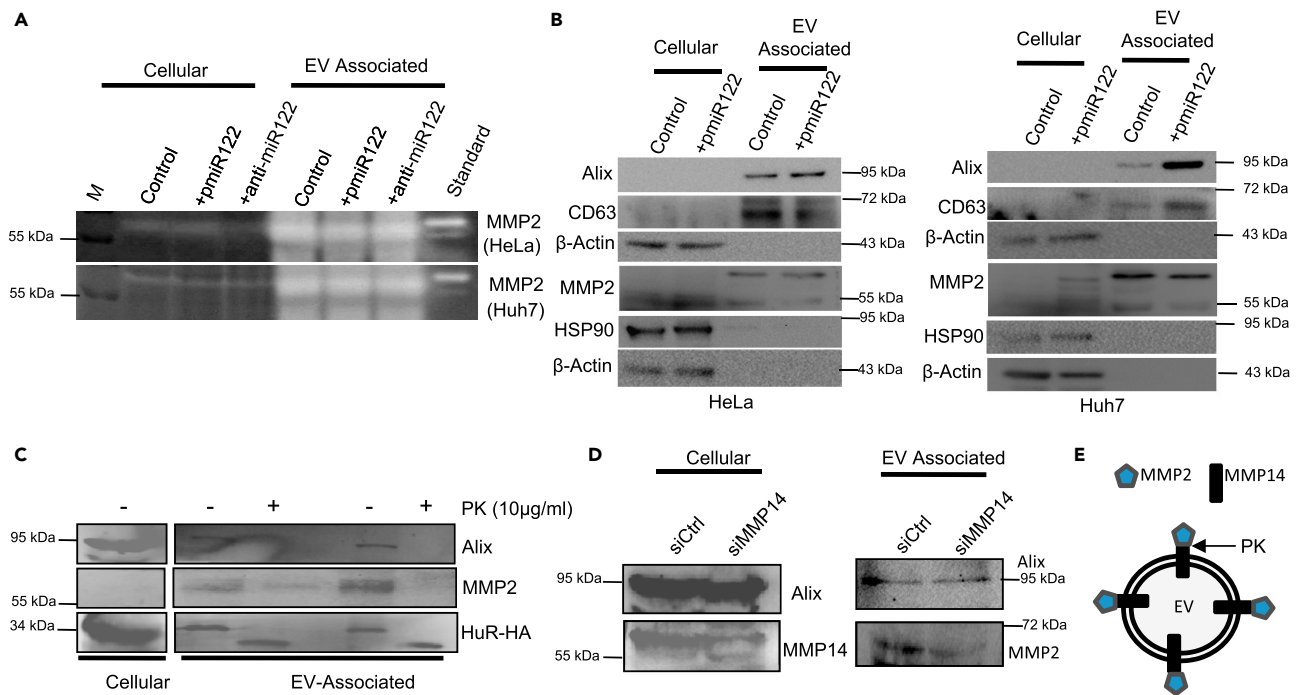


**Figure 5. Presence of MMP2 on the extracellular vesicles (EVs) isolated from different hepatic and non-hepatic cells**

(A). Gelatin zymography reveals the presence of functional MMP2 in EVs isolated from hepatic cells. Extracellular vesicles or EVs were isolated from hepatic Huh7 cells transfected with or without miR-122-expressing plasmid pmiR-122 or pCneo control plasmid. Anti-miR-122 treatment was also done in separate set cells. Cell lysates and EV extract (100 ng of protein each) were electrophoresed in 8% SDS-polyacrylamide gel containing 1 mg/mL gelatin under non-reducing conditions.

(B) Presence of MMP2 in EVs isolated from hepatic and non-hepatic cells (Huh7 and HeLa). Cells were transfected either with miR-122-expressing plasmid pmiR-122 or pCneo vector. Extract of cells or isolated EVs (100 ng of protein each) were then electrophoresed in 10% SDS-polyacrylamide gel followed by western blot analysis of the indicated proteins.

(C) Effect of proteinase K (PK) treatment (10 ng/μL) on EV-associated Alix, MMP2, and HA-HuR proteins. Isolated EVs were treated with PK for 10 min at 37°C, and after incubation, the reaction was stopped by addition of PMSF (final concentration 5 mM), extracts were analyzed on 10% SDS-PAGE and western blotted.

(D and E) Effect of MMP14 downregulation on MMP2 association with EVs. Huh7 cells were transfected with siRNAs specific to MMP14 or control siRNA and the cellular and EV associated levels of MMP14 and MMP2 were detected by western blot in the respective samples (D). A suggested model of MMP14-mediated recruitment of MMP2 to EVs (E).

See also [Figure S3](#).

### MMP2 is present on liver cell-derived EVs and its association with EVs is dependent on MMP14

Presence of MMP2 in EVs isolated from human cells has been reported before, where the MMP2 was found to promote the effect of EVs on target cells (Tang et al., 2019). We have found the presence of MMP2 in EVs isolated from liver and non-liver cells. We detected mature MMP2 in the EVs isolated from control Huh7 cells or cells expressing excess miR-122 (pmiR-122 transfected) and from Huh7 cells inactivated for miR-122 by anti-miR-122 treatment. In all these cases we detected MMP2 by gelatin zymography and by western blot (Figures 5A and 5B right panel). We also detected MMP2 by western blot in EVs derived from non-hepatic cell HeLa (Figure 5B left panel). The mature form of the MMP2 was not detected in Huh7 and HeLa cells, but mature MMP2 was predominantly found in the EVs. The EV-associated MMP2 was found to be sensitive to proteinase K treatment, and no MMP2 was detected in EVs after proteinase K treatment (Figure 5C). These results suggest the presence of MMP2 on the outer side of the EVs. MMP14 is known to retain MMP2 within the cell and EV membrane (Han et al., 2015). To explore the retention mechanism of MMP2 within EVs, we inactivated MMP14 to check the presence of MMP2 associated with EVs. Depletion of MMP14 in Huh7 cells followed by isolation of EVs and western blotting for MMP2 showed a decrease in MMP2 levels in EVs isolated from MMP14-compromised Huh7 cells (Figure 5D). Our data suggest that the presence of MMP2 on the outer side of the EV membrane is dependent on MMP14 (Figure 5E) and the MMP2 is required for intercellular EV transfer across the cell boundaries.

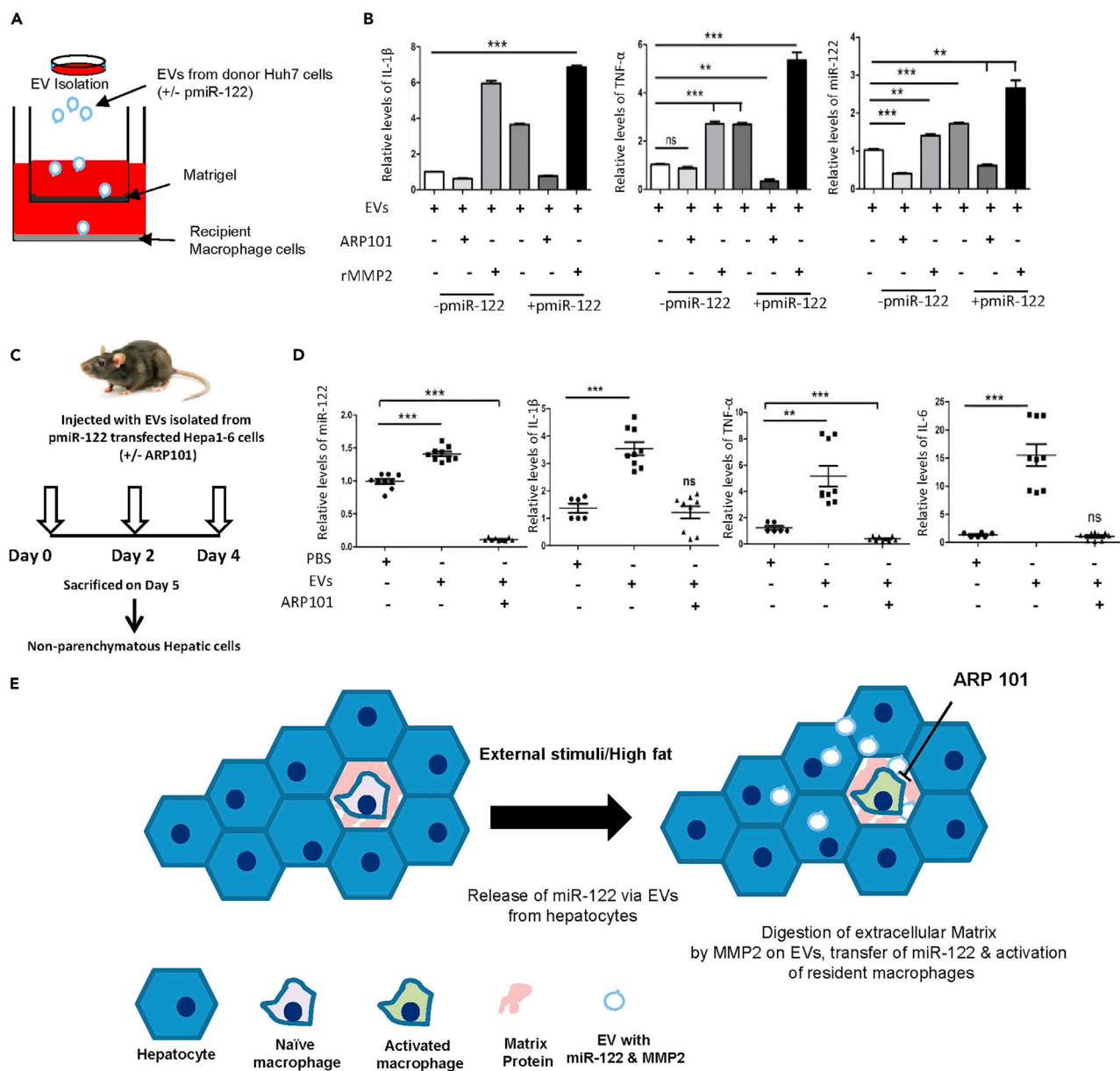


**Figure 6. Inhibition of MMP2 affects transfer of pro-inflammatory signal across the hepatic cell boundary**

(A-B) MMP2 facilitates the miR-122 transfer to macrophage that leads to elevated levels of various pro-inflammatory cytokine mRNAs. Scheme of the experiment has been shown in (A). Huh7 was transfected with control vector or pmiR-122 and EVs were isolated. Here RAW264.7 cells were taken as recipient cell. To check the transfer, Transwell inserts (0.4- $\mu$ M pore inserts, SPL) were taken and 100  $\mu$ L (3 mg/ml) diluted Matrigel was coated and solidified previously. In the lower chamber, RAW264.7 cells were seeded in complete RPMI media with 10% FCS. Then RAW264.7 cells were activated using LPS (1  $\mu$ g/ml) for 4 h. EVs were added on the inserts and incubated for 30 min at 37°C. Serum-free DMEM was added onto the inserts with ARP101 (12.5  $\mu$ M). In the control sets, the same amount of DMSO (v/v) was added. This was then incubated for 24 h. On the next day, the inserts were removed and the medium from the lower chamber was discarded and RNA was isolated by using the Trizol RNA isolation method. cDNA was synthesized followed by real-time PCR for pro-inflammatory (IL-1 $\beta$  and TNF- $\alpha$ ) cytokines and miR-122 (B).

Normalization was done with respect to 18S rRNA and U6 snRNA, respectively. Data represent mean  $\pm$  SD. (C-D) Relative internalized miR-122 levels transferred to non-parenchymatous hepatic cells in the presence and absence of ARP101. The scheme of the experiment has been shown in (C). EVs isolated from miR-122-expressing Hepa1-6 cells were injected through the tail vein every alternate day for 3 days and mice were sacrificed the day after the third injection. An equal volume of PBS was administered as the control. Non-parenchymatous hepatic cells were isolated. Low miR-122 level was detected when MMP2 inhibitor was applied. Normalization was done with respect to U6 snRNA. Data represent mean  $\pm$  SD. Cytokine mRNA levels in isolated non-parenchymatous hepatic cells have been shown here. mRNA levels were detected by RT-qPCR. Normalization was done with respect to 18S. Data represent mean  $\pm$  SD (D). N = 3 replicates.

**Figure 6. Continued**

(E) A model of EV-mediated activation of resident macrophage in liver. The miR-122-containing EVs released by activated hepatocytes digest the matrix by associated MMP2 and get transferred to non-parenchymatous hepatic cells to activate them to express the pro-inflammatory cytokines, a process that gets inhibited by ARP101, the MMP2 inhibitor. For statistical significance, minimum three independent experiments were considered in each case unless otherwise mentioned and error bars are represented as mean  $\pm$  S.E.M. p Values were calculated by using Student's t test. ns: non-significant, \*\*p < 0.01, \*\*\*p < 0.0001.

See also [Figure S4](#).

**MMP2 facilitates EV movement across extracellular matrix and also enhances EV entry in mammalian cells**

Why is MMP2 required for the EV-cargo delivery? It is possible that the presence of MMP2 on the EV surface enables them to migrate through the extracellular matrix by degrading the extracellular mesh made up of collagen and thereby ensure a faster movement of the EV across the matrix. To test that, we used a gelatin matrix prepared *in vitro* using solidified gelatin and performed a "EV-Movement" monitoring assay. We isolated EVs from hepatic cells and applied them on the well formed in the bed of the gelatin matrix and measured the movement of the EVs front for a fixed amount of time. We measured the EV movement across the matrix in the presence and absence of MMP2 inhibitor ARP101 or rMMP2. In the control and in the presence of rMMP2, we documented movement of the EV-front in collagen matrix and measured the radius of diffusion from the center. There was no specific movement of the EV front in the presence of ARP101, confirming the importance of MMP2 in the EV-movement process across the collagen matrix ([Figure S3A–S3C](#)). Does MMP2 also help in the internalization of EV? We performed the EV-uptake experiment done in 2D cell culture without having a Matrigel matrix. We noted the MMP2-dependent uptake of CD63-GFP-positive EVs in HeLa cells and the fact that the entry of CD63-GFP-positive vesicles was retarded in the presence of the MMP2 inhibitor ARP101 ([Figure S3D–S3E](#)). These data suggest a possible role of MMP2 not only in ensuring the movement of EVs across the matrix but also in its uptake in recipient cells.

**Trafficking of miRNA-containing EVs in mouse liver from hepatic cells to macrophage requires MMP2**

How does MMP2 affect the functional transfer of miRNA via EVs in a physiological context? miR-122 is a hepatocyte-derived proinflammatory miRNA that, when transferred to naive macrophage cells, can activate them. To score the effect of MMP2 inhibition on transfer of hepatic EVs to resident macrophages, we adopted a similar experimental setup as described in [Figure 3A](#) where the recipient macrophage cells were grown in the bottom chamber of a 12-well multi-well plate with insert and hepatocyte-derived EVs were added on the upper chamber that was layered with Matrigel along with DMSO or ARP101 as MMP2 inhibitor. We scored the transfer of miR-122 to recipient RAW264.7 monocytes and measured the proinflammatory cytokine levels there ([Figure 6A](#)). We have documented upregulation of proinflammatory cytokines in cells where miR-122 were also getting transferred. Interestingly, blocking of miR-122-containing EV transfer by MMP2 inhibitor also affects the proinflammatory cytokine expression there ([Figures 6A and 6B](#)). Application of MMP2 inhibitor ARP101 alone to RAW264.7 cells, however, did not show any change in expression of inflammatory cytokines compared with the DMSO control ([Figure S2F](#)). Therefore, the effect of ARP101 on cytokine expression in the presence of miR-122-containing EVs was specific to the effect that ARP101 had on EV-associated MMP2 inhibition and subsequent blocking of transfer of miR-122 via EVs to recipient cells. Like in HepG2 cells, there was no change in expression of pre-miR-122 level in RAW264.7 cells treated with miR-122-containing EVs ([Figure S2D](#)). To make a direct correlation between MMP2 and proinflammatory response in recipient RAW264.7 cells, we treated the EVs with rMMP2 and documented a positive influence of rMMP2 on miR-122 internalization and proinflammatory response induced by hepatic EVs in RAW264.7 cells ([Figure 6B](#)).

To score the *in vivo* effect of MMP2 inhibition in induction of inflammatory response by miR122-containing EVs, we expressed miR-122 in Hepa1-6 cells and isolated the EVs. The EVs were injected through the tail vein in recipient mice alone or with MMP2 inhibitor ARP101. We documented reduced levels of pro-inflammatory cytokine expression and miR-122 transfer in non-parenchymal hepatic cell population in the liver of animals injected with ARP101 ([Figures 6C and 6D](#)). Our data suggest the importance of MMP2 for intra-tissue miRNA transfer in mouse liver ([Figure 6E](#)). How does the internalized miR-122 affect the cytokine expression in resident macrophage of mouse liver? In RAW264.7 cells, either ectopic expression of miR-122 or treatment with miR-122-containing EVs led to an increase in phospho-ERK levels associated with

the activation of the NF- $\kappa$ B pathway. In miR-122-containing EV-treated cells, we noted a strong induction of phospho-NF- $\kappa$ B p65, a factor associated very much with enhanced pro-inflammatory cytokine expression (Liu et al., 2017) (Figures S4A–S4B). The application of ERK inhibitor U0126 not only prevented the phosphorylation of ERK but also reduced the expression of TNF- $\alpha$  and IL-1 $\beta$  in miR-122 EV-treated cells possibly by blocking the phosphorylation of NF- $\kappa$ B p65 (Figures S4C–S4E). However, the decrease of cytokine induction was not due to defective internalization of miR-122 in U0126-treated cells as the levels of internalized miR-122 had increased with U0126 (Figure S4F).

## DISCUSSION

In the work described above, we have identified how the matrix metalloproteinase MMP2 by facilitating the movement of EVs through the extracellular matrix affects functional miRNA transfer in the hepatic context and plays a role in liver-specific miRNA-mediated inflammation. miRNA transfer between similar or different types of cells in a tissue causes miRNA homeostasis but how miRNA expression levels are controlled by the factors that affect the transfer process per se were unknown.

EVs help in cell-to-cell communication and, like hormones, can have an autocrine, a paracrine, or an endocrine effect (Becker et al., 2016). miRNAs packaged in EVs are speculated to fine-tune the gene expression profile in neighboring cells and tissues and, thus, could facilitate metabolic and functional homeostasis in respective tissues (Chevillet et al., 2014; Lotvall and Valadi, 2007). In the current work, miR-122-enriched EVs secreted from lipid-loaded Huh7 cells have been shown to elicit a pro-inflammatory response in recipient macrophages. Is there a reciprocal effect of secreted pro-inflammatory cytokines on Huh7 cells? The released cytokines may bind to receptors on Huh7 cells and affect the transcription flux of HuR and other factors that mediate the extracellular export pathway (Mukherjee et al., 2016). Possibility of the existence of such a feedback loop could help to curb the pro-inflammatory response in recipient macrophages and could also fine-tune the miRNA profile in donor Huh7 cells and, thus, could help in the attainment of tissue-level homeostasis in gene expression. Deciphering the mechanism of such a feedback loop can be looked into in future studies. The propagation of inflammatory miR-122 as part of EVs in the blood of high-fat diet-fed mice raises the possibility of the miRNA being taken up by far located tissue macrophage in other organs where it may play a role in ectopic activation of the immune cells across the tissue boundary and, thus, contribute to a chronic systemic inflammatory response in mice exposed to high-fat diet.

MicroRNA transfer can be controlled at three different steps: the packaging and export of the miRNAs via EVs, the movement of EVs through the extracellular matrix, and internalization and release of content of EVs in the recipient cells. Exploration of all three steps is largely limited in identification of the few factors individually controlling these steps. HuR is one such protein that has been identified as the facilitator of export of specific subset of miRNAs including miR-122 from hepatic cells to ensure its export in stress conditions (Mukherjee et al., 2016). This protects the hepatic cells from stress. The effect of stress on MMP2 is known, and it also seems to have limited effect on MMP2 present on the EVs released by the hepatic cells under stress condition (data not shown). From the data described here, MMP2 expression also seems to remain unaffected in Huh7 cells at the protein level after expression of excess miR-122. miR-122 after getting into hepatic cells also decreases factors preventing its expression such as hepatic insulin-like growth factor 1 to ensure robust miR-122 expression (Basu and Bhattacharyya, 2014).

Does miR-122 directly regulate the inflammatory cytokine expression? From the previously published work by Zhang et al. (2019) it is clear that UCA1-relieved oxygen glucose deprivation-aroused H9c2 cell injury via declining miR-122 that is related to promotion of the AKT/mTOR pathway and suppression of the JNK/p38MAPK pathway. In another reported work by Manfè et al. (2012), it has been shown that miR-122 regulates p53/Akt signaling to control chemotherapy-induced apoptosis in cutaneous T cell lymphoma. Interestingly, we also had strong induction of phospho-ERK and phospho-NF- $\kappa$ B-p65 in cells receiving miR-122 via EVs, which signifies the activation of the NF- $\kappa$ B pathway by miR-122 leading to inflammatory cytokine induction. The importance of the active ERK pathway in miR-122-mediated activation and upregulation of cytokine production has been substantiated in subsequent experiments where application of ERK inhibitor U0126 has reversed the miR-122-mediated upregulation of IL-1 $\beta$  and TNF- $\alpha$  (Figure S4). Interestingly, there had been an increase in internalized miR-122 level with application of the inhibitor in RAW264.7 cells. This signifies further that miR-122 acts through the ERK pathway and there may be a halted or reduced turnover of miR-122 that is controlled by the ERK pathway. Interestingly, our

laboratory has reported previously about the lowering of miR-122 levels in the mouse liver with *Leishmania donovani* (*Ld*) infection that is associated with reduced expression of pro-inflammatory cytokine and excess expression of anti-inflammatory cytokine (Ghosh et al., 2013). Considering all these data we can conclude the causative relation of miR-122 release via EV and activation of resident and newly recruited macrophage in mouse liver by miR-122.

The role of miR-122 in the induction of inflammatory cytokines has also been explored in different context. In the report by Momen-Heravi et al. (2015) the role of miR-122 in potentiating the macrophage for LPS-induced activation has been shown whereas the report by Wang Y. et al. (2019) has described how the miR-122 from injured liver can elicit acute pulmonary inflammation via activating the alveolar macrophage TLR7 signaling pathway (Wang et al., 2019). In another work from our group, we have explored the role of EV-derived miR-122 in eliciting inflammatory cytokine expression in tissue macrophages, which get prevented by the parasite *Ld*, which targets entry of miR-122-containing EVs to stop inflammation due to mitochondrial depolarization in infected liver-resident macrophages (Ghoshal et al., 2020). Therefore, the inflammatory role of miR-122 is more obvious than anticipated, and in the context of leishmania infection, low miR-122 entry is associated with restricted expression of inflammatory cytokines. miR-122 knockout (KO) mice have problems with lipid biogenesis and therefore have problem with lipid accumulation (Tsai et al., 2012). In miR-122 KO mice, spontaneous development of hepatocellular carcinoma has also been reported (Tsai et al., 2012). Therefore, miR-122 KO animals may not be an ideal system to study the context of miR-122 effect on cytokine expression as the unrelated systematic change in liver metabolism may make it difficult to conclude the specific role of miR-122 in inflammation as the tissue may itself be inflammatory in nature owing to tumor development in miR-122 KO animal liver (Tsai et al., 2012). The longer duration of defective cholesterol biosynthesis in miR-122-depleted hepatic tissue could also contribute to the inflammatory process. In addition, in control mice liver the circulating miR-122 level is low and does not induce any inflammatory response there (Figures 1C–1F). Therefore, the requirement of miR-122 KO background to score the effect of miR-122-containing EVs is not obvious. Expression of HA-HuR, the miR-122 binder and exporter protein, actually drives the miR-122 export via EV from mouse liver and is known to cause inflammatory response in mouse liver (Goswami et al., 2020; Mukherjee et al., 2016). These data also suggest a strong connection of miR-122-containing EVs and inflammation.

According to our claim, MMP2 is recruited from the extracellular matrix to the membrane of EVs secreted by miR-122-expressing Huh7 cells. In experiments done with recombinant MMP2, it is shown that the inflammatory response, in recipient cells of EV-associated miR-122, increased several fold and, therefore, suggests a correlative relation of MMP2 and inflammation observed in the liver. In addition, the inhibitor of MMP2 has a clear effect on inflammatory cytokine production and miR-122 transfer. Interestingly, in high-fat diet-fed animal liver, MMP2 expression does not change against the normal chow-fed control group, whereas a change in several inflammatory cytokines has been detected (Table S1). However, in normal animal liver there was no substantial level of inflammatory cytokines produced as the release of miR-122 was not initiated by high lipid exposure of the donor hepatic cells. A transient application of inhibitor for MMP2 would have much less pleiotropic effect and thus act as a useful system to score MMP2's importance in miR-122 transfer to recipient macrophage cells both in *ex vivo* and *in vivo* contexts (Figures 6B and 6D). In separate experiments described in Figures S2E and S2F, we have checked the effect of MMP2 inhibitor on cytokine level and miR-122 activity change to conclude that the MMP2 inhibitor ARP101 specifically blocks miR-122 transfer to curtail inflammatory response in recipient macrophage cells.

However, considering the comparable levels of transferred miR-122 and induced TNF- $\alpha$  in recipient macrophages treated with EVs from either control Huh7 in the presence of rMMP2 or pmiR-122-transfected Huh7 without rMMP2 in culture medium, it is expected that the additional effect of rMMP2 in control EV-treated cells is because miR-122 in control Huh7 EVs compensates itself due to higher entry of the EV-containing miR-122 in the presence of MMP2 (Figure 6B). Interestingly, the CD63-positive EVs entry and Cy3-miR-122 increase in recipient cells are similarly enhanced by rMMP2 (Figures 3E and 3F). Therefore, a strong correlation if not connection exists between cellular miR-122 transfer and rMMP2 presence on EVs, both of which are enhanced when rMMP2 is applied in excess (possibly due to limited amount of MMP2 present in the matrix to facilitate the complete transfer of EVs with miR-122 to recipient cells). So, only MMP2 alone could enhance the miR-122 entry in recipient cells treated with control hepatocyte-derived EVs also. MicroRNAs, as epigenetic signals, are exchanged between neighboring cells in a functional form and ensure that they are transferred as the single-stranded form and get incorporated into the recipient cell Ago2

protein and play an important role in controlling the expression of target mRNA in both donor and recipient cells. To ensure the effective transfer of miRNAs, the movement of EVs through the matrix is an important factor, and several biochemical and physical properties of the matrix should have contributed to controlling the speed of the movement. The collagen network and extracellular proteases must work in a reciprocal manner to ensure the movement. The concentration and maturation of MMPs should be the key aspects that determine the EVs movement through the extracellular matrix. In the tumor microenvironment, the multidimensional movement of cancer cell-derived EVs contributes to the establishment of cancer cell niche by affecting the gene expression of non-cancerous and immune cells present in the tumor. Variable expression of MMPs by cancer cells is known to be essential for niche creation. We propose that MMP-mediated facilitation of the EV's movement may thus contribute to cancer progression by ensuring the rapid movement of EVs in 3D. Blocking of EV transport by targeting MMPs would thus be an effective way of controlling miRNA transport in mammalian cells and may be a useful tool to curtail cancer tumor growth.

### Limitation of the study

To make a causative connection of EV-associated miR-122 to inflammatory response observed in mouse liver, further experimental validation of *in vivo* depletion of miR-122 will be needed to show that miR-122 in EVs directly causes increased inflammatory cytokines in liver macrophages.

### STAR★METHODS

Detailed methods are provided in the online version of this paper and include the following:

- KEY RESOURCES TABLE
- RESOURCE AVAILABILITY
  - Lead contact
  - Materials availability
  - Data and code availability
- EXPERIMENTAL MODEL AND SUBJECT DETAILS
  - Cell culture
  - Animal experiments
  - Liver macrophage sorting and analysis by flow cytometry (FACS)
  - Primary hepatocyte isolation
- METHOD DETAILS
  - Plasmid constructs, cell transfections and luciferase assay
  - Cholesterol treatment
  - Inhibitor and recombinant protein treatments
  - EV isolation
  - EV injection experiment
  - RNase assay of EV associated miR-122
  - Gelatin zymography and *in vitro* EV movement assay
  - Endogenous miR-122 target mRNA quantitation
  - Quantitative estimation of mRNA and miRNA levels
  - Identification of differentially expressed MMPs and cytokines
  - Western blot analysis
  - Fluorescence microscopy
  - Post capture image analysis
- QUANTIFICATION AND STATISTICAL ANALYSIS

### SUPPLEMENTAL INFORMATION

Supplemental information can be found online at <https://doi.org/10.1016/j.isci.2021.103428>.

### ACKNOWLEDGMENTS

We thank Witold Filipowicz and Gunter Meister for different constructs used in this study. We thank the Funding body, Department of Science and Technology (DST), Govt. of India and Council for Scientific and Industrial Research (CSIR), and University Grant Commission (UGC) for the fellowship to D.B., S.Bose, S.Chakraborty, and M.A. A.D., S.Basu and D.D. also acknowledge the support from the Department of Biotechnology, Govt. of India and Department of Science and Technology (DST), Govt. of India

for their fellowship support. S.N.B. was supported by SwarnaJayanti Fellowship (DST/SJF/LSA-03/2014-15) from DST, Govt. of India and the CSIR funded Niche Creating Project RNAMEOD (MLP-139).

## AUTHOR CONTRIBUTIONS

S.N.B. conceived the idea, designed the experiments, analyzed the data, and wrote the manuscript. S.Basu, A.D., K.M., S.S., S. Chakrabarti, and P.C. contributed to design and planning the experiments. A.D. S.Basu, D.B., S.Chakraborty, D.D., and M.A. performed the experiments with the help of S.J. and S. Bose. S.Basu, A.D., D.B., and K.M. also wrote the manuscript with S.N.B. and analyzed the data.

## DECLARATION OF INTERESTS

The authors declare no conflict of interest.

Received: January 27, 2021

Revised: October 22, 2021

Accepted: November 8, 2021

Published: December 17, 2021

## REFERENCES

- Alisi, A., Carpino, G., Oliveira, F.L., Panera, N., Nobili, V., and Gaudio, E. (2017). The role of tissue macrophage-mediated inflammation on NAFLD pathogenesis and its clinical implications. *Mediators Inflamm.* 2017, 8162421. <https://doi.org/10.1155/2017/8162421>.
- Bartel, D.P. (2009). MicroRNAs: target recognition and regulatory functions. *Cell* 136, 215–233. <https://doi.org/10.1016/j.cell.2009.01.002>.
- Bartel, D.P. (2018). Metazoan MicroRNAs. *Cell* 173, 20–51. <https://doi.org/10.1016/j.cell.2018.03.006>.
- Basu, S., and Bhattacharyya, S.N. (2014). Insulin-like growth factor-1 prevents miR-122 production in neighbouring cells to curtail its intercellular transfer to ensure proliferation of human hepatoma cells. *Nucleic Acids Res.* 42, 7170–7185. <https://doi.org/10.1093/nar/gku346>.
- Becker, A., Thakur, B.K., Weiss, J.M., Kim, H.S., Peinado, H., and Lyden, D. (2016). Extracellular vesicles in cancer: cell-to-cell mediators of metastasis. *Cancer Cell* 30, 836–848. <https://doi.org/10.1016/j.ccell.2016.10.009>.
- Berg, A.H., and Scherer, P.E. (2005). Adipose tissue, inflammation, and cardiovascular disease. *Circ. Res.* 96, 939–949. <https://doi.org/10.1161/01.RES.0000163635.62927.34>.
- Bhattacharyya, S.N., Habermacher, R., Martine, U., Closs, E.I., and Filipowicz, W. (2006). Relief of microRNA-mediated translational repression in human cells subjected to stress. *Cell* 125, 1111–1124. <https://doi.org/10.1016/j.cell.2006.04.031>.
- Bose, M., and Bhattacharyya, S.N. (2016). Target-dependent biogenesis of cognate microRNAs in human cells. *Nat. Commun.* 7, 12200. <https://doi.org/10.1038/ncomms12200>.
- Caballero, F., Fernandez, A., Matias, N., Martinez, L., Fucho, R., Elena, M., Caballeria, J., Morales, A., Fernandez-Checa, J.C., and Garcia-Ruiz, C. (2010). Specific contribution of methionine and choline in nutritional nonalcoholic steatohepatitis: impact on mitochondrial S-adenosyl-L-methionine and glutathione. *J. Biol. Chem.* 285, 18528–18536. <https://doi.org/10.1074/jbc.M109.099333>.
- Cai, D., Yuan, M., Frantz, D.F., Melendez, P.A., Hansen, L., Lee, J., and Shoelson, S.E. (2005). Local and systemic insulin resistance resulting from hepatic activation of IKK-beta and NF-kappaB. *Nat. Med.* 11, 183–190. <https://doi.org/10.1038/nm1166>.
- Chang, J., Nicolas, E., Marks, D., Sander, C., Lerro, A., Buendia, M.A., Xu, C., Mason, W.S., Moloshok, T., Bort, R., et al. (2004). miR-122, a mammalian liver-specific microRNA, is processed from hcr mRNA and may downregulate the high affinity cationic amino acid transporter CAT-1. *RNA Biol.* 1, 106–113.
- Chevillet, J.R., Kang, Q., Ruf, I.K., Briggs, H.A., Vojtech, L.N., Hughes, S.M., Cheng, H.H., Arroyo, J.D., Meredith, E.K., Gallichotte, E.N., et al. (2014). Quantitative and stoichiometric analysis of the microRNA content of exosomes. *Proc. Natl. Acad. Sci. U S A* 111, 14888–14893. <https://doi.org/10.1073/pnas.1408301111>.
- Esau, C., Davis, S., Murray, S.F., Yu, X.X., Pandey, S.K., Pear, M., Watts, L., Booten, S.L., Graham, M., McKay, R., et al. (2006). miR-122 regulation of lipid metabolism revealed by in vivo antisense targeting. *Cell Metab.* 3, 87–98. <https://doi.org/10.1016/j.cmet.2006.01.005>.
- Filipowicz, W., Bhattacharyya, S.N., and Sonenberg, N. (2008). Mechanisms of post-transcriptional regulation by microRNAs: are the answers in sight? *Nature reviews. Genetics* 9, 102–114. <https://doi.org/10.1038/nrg2290>.
- Ghosh, J., Bose, M., Roy, S., and Bhattacharyya, S.N. (2013). Leishmania donovani targets Dicer1 to downregulate miR-122, lower serum cholesterol, and facilitate murine liver infection. *Cell Host Microbe* 13, 277–288. <https://doi.org/10.1016/j.chom.2013.02.005>.
- Ghoshal, B., Bertrand, E., and Bhattacharyya, S.N. (2020). Non-Canonical ago loading of EV-derived exogenous miRNA generates foreign miRNPs on endosomes to arbitrate gene expression in recipient cells. *bioRxiv*. <https://doi.org/10.1101/2020.05.26.115899>.
- Ghoshal, B., Bertrand, E., and Bhattacharyya, S.N. (2021). Non-canonical ago loading of EV-derived exogenous single stranded miRNA in recipient cells. *J. Cel. Sci.* <https://doi.org/10.1242/jcs.253914>.
- Goswami, A., Mukherjee, K., Mazumder, A., Ganguly, S., Mukherjee, I., Chakrabarti, S., Roy, S., Sundar, S., Chattopadhyay, K., and Bhattacharyya, S.N. (2020). MicroRNA exporter HuR clears the internalized pathogens by promoting pro-inflammatory response in infected macrophages. *EMBO Mol. Med.* 12, e11011. <https://doi.org/10.15252/emmm.201911011>.
- Han, K.Y., Dugas-Ford, J., Seiki, M., Chang, J.H., and Azar, D.T. (2015). Evidence for the involvement of MMP14 in MMP2 processing and recruitment in exosomes of corneal fibroblasts. *Invest. Ophthalmol. Vis. Sci.* 56, 5323–5329. <https://doi.org/10.1167/iovs.14-14417>.
- Han, L., Sheng, B., Zeng, Q., Yao, W., and Jiang, Q. (2020). Correlation between MMP2 expression in lung cancer tissues and clinical parameters: a retrospective clinical analysis. *BMC Pulm. Med.* 20, 283. <https://doi.org/10.1186/s12890-020-01317-1>.
- Jo, Y.K., Park, S.J., Shin, J.H., Kim, Y., Hwang, J.J., Cho, D.H., and Kim, J.C. (2011). ARP101, a selective MMP-2 inhibitor, induces autophagy-associated cell death in cancer cells. *Biochem. Biophys. Res. Commun.* 404, 1039–1043. <https://doi.org/10.1016/j.bbrc.2010.12.106>.
- Jopling, C. (2012). Liver-specific microRNA-122: biogenesis and function. *RNA Biol.* 9, 137–142. <https://doi.org/10.4161/rna.18827>.
- Kundu, P., Fabian, M.R., Sonenberg, N., Bhattacharyya, S.N., and Filipowicz, W. (2012). HuR protein attenuates miRNA-mediated repression by promoting miRISC dissociation from the target RNA. *Nucleic Acids Res.* 40, 5088–5100. <https://doi.org/10.1093/nar/gks148>.
- Liu, T., Zhang, L., Joo, D., and Sun, S.C. (2017). NF-kappaB signaling in inflammation. *Signal Transduct. Target. Ther.* 2017. <https://doi.org/10.1038/sigtrans.2017.23>.

Lotvall, J., and Valadi, H. (2007). Cell to cell signalling via exosomes through esRNA. *Cell Adh. Migr.* 1, 156–158.

Manfe, V., Biskup, E., Rosbjerg, A., Kamstrup, M., Skov, A.G., Lerche, C.M., Lauenborg, B.T., Odum, N., and Gniadecki, R. (2012). miR-122 regulates p53/Akt signalling and the chemotherapy-induced apoptosis in cutaneous T-cell lymphoma. *PLoS One* 7, e29541. <https://doi.org/10.1371/journal.pone.0029541>.

Momen-Heravi, F., Bala, S., Kodys, K., and Szabo, G. (2015). Exosomes derived from alcohol-treated hepatocytes horizontally transfer liver specific miRNA-122 and sensitize monocytes to LPS. *Scientific Rep.* 5, 9991. <https://doi.org/10.1038/srep09991>.

Morinaga, H., Mayoral, R., Heinrichsdorff, J., Osborn, O., Franck, N., Hah, N., Walenta, E., Bandyopadhyay, G., Pessentheiner, A.R., Chi, T.J., et al. (2015). Characterization of distinct subpopulations of hepatic macrophages in HFD/obese mice. *Diabetes* 64, 1120–1130. <https://doi.org/10.2337/db14-1238>.

Mukherjee, K., Ghoshal, B., Ghosh, S., Chakrabarty, Y., Shwetha, S., Das, S., and Bhattacharyya, S.N. (2016). Reversible HuR-microRNA binding controls extracellular export of miR-122 and augments stress response. *EMBO Rep.* 17, 1184–1203. <https://doi.org/10.15252/embr.201541930>.

Pillai, R.S., Bhattacharyya, S.N., Artus, C.G., Zoller, T., Cougot, N., Basyuk, E., Bertrand, E., and Filipowicz, W. (2005). Inhibition of translational

initiation by Let-7 MicroRNA in human cells. *Science* 309, 1573–1576. <https://doi.org/10.1126/science.1115079>.

Pirola, C.J., Fernandez Gianotti, T., Castano, G.O., Mallardi, P., San Martino, J., Mora Gonzalez Lopez Ledesma, M., Flichman, D., Mirshahi, F., Sanyal, A.J., and Sookoian, S. (2015). Circulating microRNA signature in non-alcoholic fatty liver disease: from serum non-coding RNAs to liver histology and disease pathogenesis. *Gut* 64, 800–812. <https://doi.org/10.1136/gutjnl-2014-306996>.

Shimoda, M., and Khokha, R. (2017). Metalloproteinases in extracellular vesicles. *Biochim. Biophys. Acta. Molecul. Cell Res.* 1864, 1989–2000. <https://doi.org/10.1016/j.bbamcr.2017.05.027>.

Shoelson, S.E., Lee, J., and Goldfine, A.B. (2006). Inflammation and insulin resistance. *J. Clin. Invest.* 116, 1793–1801. <https://doi.org/10.1172/JCI29069>.

Tan, Y., Ge, G., Pan, T., Wen, D., and Gan, J. (2014). A pilot study of serum microRNAs panel as potential biomarkers for diagnosis of nonalcoholic fatty liver disease. *PLoS one* 9, e105192. <https://doi.org/10.1371/journal.pone.0105192>.

Tang, H., He, Y., Li, L., Mao, W., Chen, X., Ni, H., Dong, Y., and Lyu, F. (2019). Exosomal MMP2 derived from mature osteoblasts promotes angiogenesis of endothelial cells via VEGF/Erk1/2 signaling pathway. *Exp. Cel. Res.* 383, 111541. <https://doi.org/10.1016/j.yexcr.2019.111541>.

Tsai, W.C., Hsu, S.D., Hsu, C.S., Lai, T.C., Chen, S.J., Shen, R., Huang, Y., Chen, H.C., Lee, C.H., Tsai, T.F., et al. (2012). MicroRNA-122 plays a critical role in liver homeostasis and hepatocarcinogenesis. *J. Clin. Invest.* 122, 2884–2897. <https://doi.org/10.1172/JCI63455>.

Valadi, H., Ekstrom, K., Bossios, A., Sjostrand, M., Lee, J.J., and Lotvall, J.O. (2007). Exosome-mediated transfer of mRNAs and microRNAs is a novel mechanism of genetic exchange between cells. *Nat. Cel. Biol.* 9, 654–659. <https://doi.org/10.1038/ncb1596>.

Wang, B., Ding, Y.M., Fan, P., Xu, J.H., and Wang, W.X. (2014). Expression and significance of MMP2 and HIF-1alpha in hepatocellular carcinoma. *Oncol. Lett.* 8, 539–546. <https://doi.org/10.3892/ol.2014.2189>.

Wang, Y., Liang, H., Jin, F., Yan, X., Xu, G., Hu, H., Liang, G., Zhan, S., Hu, X., Zhao, Q., et al. (2019). Injured liver-released miRNA-122 elicits acute pulmonary inflammation via activating alveolar macrophage TLR7 signaling pathway. *Proc. Natl. Acad. Sci. USA* 116, 6162–6171. <https://doi.org/10.1073/pnas.1814139116>.

Zhang, Z., Li, H., Cui, Z., Zhou, Z., Chen, S., Ma, J., Hou, L., Pan, X., and Li, Q. (2019). Long non-coding RNA UCA1 relieves cardiomyocytes H9c2 injury aroused by oxygen-glucose deprivation via declining miR-122. *Artif. Cell Nanomed. Biotechnol.* 47, 3492–3499. <https://doi.org/10.1080/21691401.2019.1652630>.

**STAR★METHODS**

**KEY RESOURCES TABLE**

REAGENT or RESOURCE	SOURCE	IDENTIFIER
<b>Antibodies</b>		
Rabbit monoclonal anti-MMP2	Cell Signaling Technology	Cat# 13132; RRID:AB_2798128
Mouse monoclonal anti-Alix	Santa Cruz Biotechnology	Cat# sc-53538; RRID:AB_673821
Mouse monoclonal anti-CD63	BD Biosciences	Cat# 556019; RRID:AB_396297
Rabbit monoclonal anti-HSP90	Cell Signaling Technology	Cat# 4877; RRID:AB_2233307
Rat monoclonal anti-HA high affinity	Roche	Cat# 11867423001; RRID:AB_390918
Rabbit monoclonal anti-MMP14	Cell Signaling Technology	Cat# 13130; RRID:AB_2798127
Rabbit monoclonal anti-Phospho-p44/42 MAPK Erk1/2	Cell Signaling Technology	Cat# 4370; RRID:AB_2315112
Rabbit monoclonal anti-Phospho-NF-κB p65	Cell Signaling Technology	Cat# 3033; RRID:AB_331284
Mouse monoclonal anti-GAPDH	Sigma-Aldrich	Cat# G8795; RRID:AB_1078991
Mouse monoclonal anti-beta-Tubulin	Sigma-Aldrich	Cat# T5201; RRID:AB_609915
Mouse Monoclonal anti-beta-Actin, Horseradish Peroxidase conjugated	Sigma-Aldrich	Cat# A3854; RRID:AB_262011
Goat anti-Mouse IgG (H+L) Secondary Antibody, HRP conjugated	Thermo Fisher Scientific	Cat# 62-6520; RRID:AB_2533947
Goat anti-Rabbit IgG (H+L) Secondary Antibody, HRP conjugated	Thermo Fisher Scientific	Cat# 65-6120; RRID:AB_2533967
Goat anti-Rat IgG (H+L) Secondary Antibody, HRP conjugated	Thermo Fisher Scientific	Cat# 62-9520; RRID:AB_2533965
Goat anti-Mouse IgG (H+L) Highly Cross-Adsorbed Secondary Antibody, Alexa Fluor 488	Thermo Fisher Scientific	Cat# A-11029; RRID:AB_2534088
Goat anti-Mouse IgG (H+L) Highly Cross-Adsorbed Secondary Antibody, Alexa Fluor 568	Thermo Fisher Scientific	Cat# A-11031; RRID:AB_144696
F4/80 Monoclonal Antibody, FITC conjugated	eBioscience™, Thermo Fisher Scientific	Cat# 11-4801-82; RRID:AB_2637191
CD11b Monoclonal Antibody, APC conjugated	eBioscience™, Thermo Fisher Scientific	Cat# 17-0112-82; RRID:AB_469343
<b>Chemicals, peptides, and recombinant proteins</b>		
ARP 101	Sigma-Aldrich	Cat# A8356-25MG
U0126	Cell Signaling Technology	Cat #9903
Recombinant Human MMP-2	Calbiochem	Cat# PF037
Methionine /Choline Deficient Diet	MP Biomedicals	Cat# 0296043910
Matrigel® Growth Factor Reduced (GFR) Basement Membrane Matrix	Corning	Cat# 354230
<b>Critical commercial assays</b>		
TaqMan™ MicroRNA Reverse Transcription Kit	Applied Biosystems™	Cat# 4366597
TaqMan™ Universal PCR Master Mix, no AmpErase™ UNG	Applied Biosystems™	Cat# 4324018
Reverse Transcriptase Core kit	Eurogentec	Cat# RT-RTCK-03
MESA GREEN qPCR MasterMix Plus for SYBR® Assay Low ROX	Eurogentec	Cat# RT-SY2X-03+WOULR
Dual-Luciferase® Reporter Assay System	Promega	Cat# E1980

(Continued on next page)

<b>Continued</b>		
REAGENT or RESOURCE	SOURCE	IDENTIFIER
<b>Deposited data</b>		
Expression profiling by array	NCBI GEO Database	GSE163918
Expression profiling by array	NCBI GEO Database	GSE27713
Expression profiling by array	NCBI GEO Database	GSE31453
<b>Experimental models: Cell lines</b>		
Huh7	(Bhattacharyya et al., 2006)	N/A
HepG2	ATCC	Cat# HB-8065
Hepa1-6	ATCC	Cat# CRL-1830
HeLa	ATCC	Cat# CCL-2
RAW264.7	ATCC	Cat# TIB-71
U-937	ATCC	Cat# CRL-1593.2
<b>Experimental models: Organisms/strains</b>		
C57BL/6 mice (8-10 weeks age)	CSIR-IICB animal house	N/A
Adult BALB/c mice (4-6 weeks age)	CSIR-IICB animal house	N/A
<b>Oligonucleotides</b>		
RT-qPCR primers	This paper	See Table S2
RNA sequences	This paper	See Table S3
<b>Recombinant DNA</b>		
pmiR-122	(Chang et al., 2004)	N/A
Encoding pre-miR-122 under a constitutive U6 promoter		
imiR-122	(Bose and Bhattacharyya, 2016)	N/A
Pre-miR-122 sequence cloned within pTRE-Tight-BI Vector in NheI and NotI sites		
CD63-GFP	(Ghoshal et al., 2021)	N/A
Expressing GFP tagged CD63		
pRL-con	(Pillai et al., 2005)	N/A
Encoding humanized Renilla Luciferase coding region.		
pRL-per-miR-122	(Bhattacharyya et al., 2006)	N/A
One miR-122 perfect complementary binding sites downstream of Renilla Luciferase (RL) coding region.		
pGL3FF	Promega	N/A
Encoding Firefly Luciferase (FL) under SV40 promoter		
HA-HuR	(Kundu et al., 2012)	N/A
Expressing HA tagged HuR protein cloned in pCleo vector		
<b>Software and Algorithms</b>		
Prism 5	GraphPad	<a href="http://www.graphpad.com/">http://www.graphpad.com/</a> ; RRID:SCR_002798
Zen Blue	Zeiss	<a href="http://www.zeiss.com/microscopy/en_us/products/microscope-software/zen.html#introduction">http://www.zeiss.com/microscopy/en_us/products/microscope-software/zen.html#introduction</a> ;RRID:SCR_013672
Imaris7	Bitplane	<a href="http://www.bitplane.com/imaris/imaris">http://www.bitplane.com/imaris/imaris</a> ; RRID:SCR_007370

(Continued on next page)

**Continued**

REAGENT or RESOURCE	SOURCE	IDENTIFIER
<i>Other</i>		
Liver Digest Medium	(Gibco™) Thermo Fischer Scientific	Cat#17703034
Hepatocyte Wash Medium	(Gibco™) Thermo Fischer Scientific	Cat#17704024
Collagen I, Rat Tail	(Gibco™) Thermo Fischer Scientific	Cat# A1048301
HepatoZYME-SFM	(Gibco™) Thermo Fischer Scientific	Cat# 17705021
Hank's Balanced Salt Solution (HBSS)	(Gibco™) Thermo Fischer Scientific	Cat# 14175095
Liver perfusion Medium 1x	(Gibco™) Thermo Fischer Scientific	Cat# 17701038
Fetal Bovine Serum, certified, heat inactivated, United States	(Gibco™) Thermo Fischer Scientific	Cat# 10082147
DMEM, powder, high glucose, pyruvate	(Gibco™) Thermo Fischer Scientific	Cat# 12800017
RPMI 1640 Medium, powder	(Gibco™) Thermo Fischer Scientific	Cat# 31800022
Trypsin-EDTA (0.25%), phenol red	(Gibco™) Thermo Fischer Scientific	Cat# 25200072

## RESOURCE AVAILABILITY

### Lead contact

Further information and requests for resources and reagents should be directed to and will be fulfilled by the Lead Contact, Dr. Suvendra N. Bhattacharyya ([suvendra@iicb.res.in](mailto:suvendra@iicb.res.in)).

### Materials availability

This study did not generate new unique reagents.

### Data and code availability

- All data reported in this paper will be shared by the lead contact upon request.
- This paper does not report original code.
- Any additional information required to reanalyze the data reported in this paper is available from the lead contact upon request.

## EXPERIMENTAL MODEL AND SUBJECT DETAILS

### Cell culture

Human HCC cell lines (Huh7, HepG2, Hepa1-6) and Human HeLa cells were cultured in Dulbecco's modified Eagle's medium (DMEM; Gibco-BRL) supplemented with 10% fetal bovine serum (FBS; GIBCO-BRL) and Penicillin Streptomycin (1X) antibiotics (GIBCO). RAW264.7 were cultured in RPMI (Gibco-BRL) supplemented with 10% fetal bovine serum (FBS; GIBCO-BRL) and Penicillin Streptomycin (1X) antibiotics (GIBCO). All cells were grown in incubator maintained at 5% CO<sub>2</sub> and 37°C temperature in a humidified atmosphere.

### Animal experiments

All animal experiments were approved by the Institutional Animal Ethics Committee (approved by CPCSEA, Ministry of Environment & Forest, and Government of India). 8-10 weeks old male (20-24g) C57BL/6 mice were housed under controlled conditions (temperature 23 ± 2°C, 12 hour/12-hour light/dark cycle) in individually ventilated cages. Mice were randomly divided into two groups and fed either standard chow diet or methionine and choline deficient diet MCD (MP Biomedicals; #0296043910) up to four weeks.

C57BL/6 male mice of 8-10 weeks age were divided in two groups for normal chow and high fat diet (HFD) containing 45% fat and 5.81 kcal/gm diet energy content (MP Biomedicals; # 960192). Animals were fed with HFD for 4 weeks.

For isolation of RNA from tissues, TRIzol® (Invitrogen) reagent was used. For analysis of EV-associated RNA, serum fraction of blood was used. Relative levels of miRNA and mRNA in serum and tissues were quantified by qRT-PCR.

For histological analysis, tissues were fixed in 10% formaldehyde in PBS, embedded in paraffin, sectioned at 10 µm, and stained with hematoxylin and eosin (H&E) following standard staining protocol.

### Liver macrophage sorting and analysis by flow cytometry (FACS)

Animals were anaesthetized and livers were slowly perfused initially with the HBSS and then with 0.05% collagenase buffer via the portal vein. Livers were then excised, minced and filtered through a 70µm cell strainer. The resultant single cell suspension was centrifuged at 250 g for 5 minutes to obtain non parenchymal cells and on the basis of surface staining with anti-F4/80 (FITC), anti-CD11b (APC) (eBioscience) antibodies, three types of liver macrophages were sorted by FACS (Beckman Coulter). CD11b+, F4/80+ and Cd11b+F4/80+ cells were sorted. Unstained cells were used for setting compensation and gates.

### Primary hepatocyte isolation

Animals were obtained from the animal house of the institute and all experiments were performed according to the guidelines set by Institutional Animal Ethics committee following the Govt. of India regulations. Mouse primary hepatocytes were isolated using the hepatocyte product line from Gibco Invitrogen Corporation. Adult BALB/c mice (4-6 weeks) were anaesthetized and the portal vein was cannulated using a 25G butterfly cannula and an incision was made in the inferior vena cava. The liver was perfused with 350 mL of warm (37°C) Liver Perfusion Medium (Cat. No. 17701) at a rate of 35 mL/minute with the perfusate exiting through the severed vena cava. This was followed by a Collagenase-Dispase digestion with Liver Digest Medium (Cat no. 17703) at a rate of 35 mL/minute. The liver was then aseptically transferred to the tissue culture hood on ice in Hepatocyte Wash Medium (cat no. 17704). Using blunt forceps the digested liver was torn open to release the hepatocytes. Cell clumps were dissociated by gently pipetting the solution up and down using a 25ml pipette. The solution was then filtered through 100 µm nylon caps atop 50 ml conical tubes. The cell suspension was then centrifuged at 50 x g for 3 min. The pellet was gently resuspended in 10 ml of Wash Medium using 25 ml pipette and the centrifugation repeated.

Cells were finally resuspended in Hepatocyte Wash Medium with 10% FCS and plated at  $1 \times 10^7$  cells/ml. Cells were plated in tissue culture treated collagen (Gibco Cat. No. A10483-01) coated plates at  $12.5 \mu\text{g}/\text{cm}^2$ . Unattached cells were poured off 4h after plating and medium was replaced with Hepatozyme-SFM (Cat no. 17705) with glutamine and 1% Pen/Strep. Cholesterol was added the next day in Hepatozyme-SFM.

For Kupffer cell isolation, supernatant obtained from the first centrifugation (at 50x g for 3 minutes) after filtering through the 100 µm cell strainer was further centrifuged at 250xg for 5 min. The cell pellet was washed, resuspended in DMEM with 10% FBS, seeded onto tissue culture plates, and allowed to adhere for 16 h. Nonadherent cells were removed by several washes with PBS; >80% adherent cells were found to be positive for F4/80, a well-established KC marker.

## METHOD DETAILS

### Plasmid constructs, cell transfections and luciferase assay

The RL reporters (Renilla luciferase) were previously described (Pillai et al., 2005).

siControl, siMMP2 and cy3-miR-122 were used for transfection at 100 pmoles per well of a confluent six-well plate. miR-122 and anti-miR-122 were purchased from Ambion and was used at 100 pmoles to transfect cells per well of a six-well plate. Cells were differentially transfected for microscopy using CD63-GFP, Tubulin-GFP 2 plasmids. For transfections 1µg of the plasmids was used for transfecting  $10^6$  cells in a  $10\text{cm}^2$  well. All transfections were performed using Lipofectamine 2000 (Invitrogen) following manufacturer's instructions. For RAW264.7 cells Fugene HD transfection reagent (Promega) was used.

For luciferase assays  $10^6$  cells in a  $10\text{cm}^2$  well were transfected with either RL-con or RL-per-miR-122 plasmids in parallel sets. To detect fold repression in HepG2,  $10^6$  cells in a  $10\text{cm}^2$  well were transfected with 150 ng of each of the plasmids. Normalisation was done with a Firefly (FF) luciferase construct which was co-transfected along with

the RL constructs ( $1\mu\text{g}$  for  $1 \times 10^6$  cells). After 24 h of transfection, cells were split, followed by incubation with EVs as indicated. Post incubation with EVs for 24 hours, cells were lysed with 1X Passive Lysis Buffer (Promega). Renilla (RL) and Firefly (FL) activities were measured using a Dual-Luciferase Assay Kit (Promega) following the suppliers protocol on a VICTOR X3 Plate Reader with injectors (Perkin Elmer). Mean Fold Repression was calculated by dividing the FF normalized RL-Con value with that of FF normalized RL-per-miR-122 value. Relative fold repression was calculated by taking the control mean fold repression as 1. All luciferase assays used in this study have been done in triplicate. All experiments were performed minimum three times before the SD values were calculated.

### Cholesterol treatment

M $\beta$ CD conjugated cholesterol conjugate obtained from GIBCO (#12531-018) was added from a 250X stock to Huh7/transfected Hepa1-6/ murine primary hepatocyte cells in culture at a final concentration of 5X for a period of 4 hours. Cholesterol treatments were done in fresh growth media at 70-80% confluency. Unless otherwise mentioned, cholesterol treatment was done at a final concentration of 5x for 4 hours.

### Inhibitor and recombinant protein treatments

MMP2 inhibitor, ARP101 was purchased from Sigma-Aldrich; recombinant MMP2 was purchased from Calbiochem. Either ARP101 ( $12.5\mu\text{M}/\text{well}$ ) or recombinant MMP2 were added onto Matrigel coated transwell inserts in serum free DMEM to score for the effect of MMP2 in modulating the transfer of EVs from donor to recipient cells through the Matrigel.

ErK inhibitor U0126 (Catalog no.: #9903) was purchased from Cell Signaling Technology and re-suspended in DMSO. To inhibit ERK, recipient RAW264.7 cells grown in 12-well plate format were pre-treated with U0126 at a final concentration of  $10\mu\text{M}$  for 2 hours prior to incubation with EVs. For control, equivalent amount of DMSO was pre-treated to recipient RAW264.7 cells.

### EV isolation

For EV isolation cells were grown in media made from EV depleted FCS which were prepared by ultracentrifugation of the FCS used at  $110,000 \times g$  for 5 h. The supernatant conditioned medium (CM) from one  $60\text{ cm}^2$  plates, having  $6 \times 10^6$  donor cells (Huh7/ transfected Hepa1-6/ murine primary hepatocytes) was taken. The CMs were centrifuged first at  $300 \times g$  for 10 min, then at  $2000 \times g$  for 15 min followed by centrifugation at  $10,000 \times g$  for 30 min. All centrifugations were done at  $4^\circ\text{C}$ . The CM was then filtered through a  $0.22\mu\text{m}$  filter unit. This was then centrifuged at  $100,000 \times g$  for 90 min at  $4^\circ\text{C}$ . After centrifugation, the supernatant was discarded. The pellet was resuspended in media and added back to recipient cells (HepG2/ RAW 264.7/ U937/ murine primary macrophages) in a 24-well format such that  $1 \times 10^5$  recipient cells received the EVs from  $1 \times 10^6$  donor cells. For CM based assays the same ratio was followed with CM from  $10^6$  cells being added to  $2 \times 10^5$  cells. For the isolation of miR-122, anti-miR-122, Huh7, HeLa and HepG2 carrying EVs,  $1 \times 10^6$  cells were transfected and 24 h after transfection, the cells were reseeded onto a  $90\text{ cm}^2$  plate. Cells were grown for 48–72 h and EVs isolated from the CM of these cells. For the EV protein isolation experiment, the CMs were centrifuged first at  $300 \times g$  for 10 mins, then at  $2000 \times g$  for 15 min followed by centrifugation at  $10,000 \times g$  for 30 mins. All centrifugations were done at  $4^\circ\text{C}$ . The CM was then filtered through a  $0.22\mu\text{m}$  filter unit and was loaded on a sucrose cushion (1 M sucrose and 10 mM Tris-HCl pH 7.5). This was ultracentrifuged at  $120,000 \times g$  for 90 mins at  $4^\circ\text{C}$ . The medium above the sucrose cushion was discarded leaving behind a narrow layer of medium with the EVs at the interface. 1X PBS was added and the separated EVs were washed at  $4^\circ\text{C}$  for 90 mins at  $100,000 \times g$ . The pellet was resuspended in  $200\mu\text{l}$  of 1X Passive Lysis Buffer (Promega), followed by protein extraction using chloroform-methanol, which was then used for western analysis for EV markers.

### EV injection experiment

For EV injection experiments, Hepa1-6 cells were transfected with miR-122 expressing plasmids ( $6\mu\text{g}/6 \times 10^6$  cells). Approximately  $1 \times 10^9$  EVs (measured by Nanoparticle Tracking Analysis- Nanosight Malvern U.K.) isolated from transfected Hepa1-6 cells ( $\sim 1 \times 10^7$  cells) were suspended in 1x PBS (passed through  $0.22\mu\text{m}$  filter units in  $100\mu\text{l}$ ) and injected into the tail vein of BALB/c mice (adult, 8-10 weeks). Control mice were injected with equal volume of 1x PBS (passed through  $0.22\mu\text{m}$  filter units). Experiment was performed with 5 mice in each group (control injected and EV injected). Injections were repeated every alternate day for three days and mice sacrificed the next day after the third injection. Animals were

anaesthetized and livers were slowly perfused initially with the HBSS and then with 0.05% collagenase buffer via the portal vein. Livers were then excised, minced and filtered through a 70  $\mu\text{m}$  cell strainer. The resultant single cell suspension was centrifuged at 50Xg for 5 minutes to precipitate and remove the hepatocytes. The supernatant was then collected and centrifuged at 250g for 15 minutes. The pellet was resuspended in RBC lysis buffer and kept in ice for 10 minutes. The resultant cell suspension was again centrifuged at 250xg for 15 minutes and pellet obtained was lysed with Trizol reagent. For detection of serum miRNA levels, serum fraction of blood was used. Blood samples were collected by cardiac puncture and allowed to clot. Serum was separated by centrifugation and frozen at  $-80^{\circ}\text{C}$ .

### RNAse assay of EV associated miR-122

To assess the spatial orientation of EV associated miR-122, i.e. whether EV associated miR-122 is present on the outer membrane of EVs or inside the EV lumen, an RNAse assay was performed. Huh7 cells were initially transfected with miR-122 expressing plasmid (pmiR-122) in a 60 mm cell culture dish. Transfected cells were split onto 90 mm dish after 24 h and grown in exosome-depleted media overnight. EVs were isolated from culture supernatants of one such 90 mm dish ( $\sim 6 \times 10^6$  cells equivalent media) by a two-step ultracentrifugation. Isolated EVs were re-suspended in ice-cold PBS and subjected to RNAse digestion in 100  $\mu\text{l}$  reaction mixture (containing 10  $\mu\text{g}$  of RNAse A [Fermentas]) at  $30^{\circ}\text{C}$  for 60 min in presence or absence of 1% Triton X-100. After reaction, RNA was extracted using Trizol LS reagent following manufacturer's protocol and miR-122 levels were detected by qRT-PCR.

### Gelatin zymography and *in vitro* EV movement assay

Human HCC cells (Huh7 and HepG2) and a non hepatic cell line HeLa were transfected with miR122 expressing plasmid pmiR-122 and anti-miR122 oligonucleotides, media was changed after 6 hours and incubated for over night at  $37^{\circ}\text{C}$  humidified incubator. Cells were split to 90 mm culture dishes containing DMEM with 2% Exo depleted FCS and kept for 24 hrs at incubator. EVs were isolated and EDTA free protease inhibitor cocktail containing lysis buffer was added to isolated EVs and 8% gelatin containing SDS-PAGE gel was run at 60v for 3 hrs. After the completion of the run gels were washed for 1hr in 2.5x Triton X and then gels were incubated in calcium assay buffer (40 mM Tris-HCl, pH 7.4, 0.2 M NaCl, 10 mM  $\text{CaCl}_2$ ) for o/n at  $37^{\circ}\text{C}$  incubator. After incubation in buffer, gels were stained with 0.1% coomassie blue and then destaining was followed. The zones of gelatinolytic activities appeared as negative staining. Images of zymographic bands were performed using an UVP BioImager 600 system equipped with VisionWorks Life Science software (UVP) V6.80.

For the diffusion rate measurement assay, Huh7 released EVs were pretreated with rMMP2 or ARP101. EVs were isolated from culture supernatant of Huh7 cells ( $1 \times 10^7$  Cells) and were then spotted on a well formed in the middle of a 35mm Petri dish layered with 2mm thick gelatine matrix. After 30 minutes the reaction was stopped by placing the gel in calcium assay buffer before they placed in for staining with Brilliant Blue to visualize the diffusion front of the EVs through the matrix. The representative plate photographs were taken and distance travelled by the MMP2 containing EVs were measured from the centre by visualizing and measuring the distance of the front visible in individual cases.

### Endogenous miR-122 target mRNA quantitation

To investigate whether the EV-mediated transfer of miR-122 to recipient RAW264.7 cells were functional or not, cellular transcript levels of endogenous miR-122 targets, namely, Cationic Amino acid Transporter 1 (CAT-1) and Aldolase A (Aldo A) in recipient RAW264.7 cells (incubated with EVs derived from pmiR-122 transfected Huh7 cells) were analyzed by qRT-PCR. Normalization was done using GAPDH mRNA levels.

### Quantitative estimation of mRNA and miRNA levels

RNA was extracted by using the TRIzol reagent according to the manufacturer's protocol (Invitrogen). Real time analyses by two-step RT-qPCR was performed for quantification of miRNA and mRNA levels. All mRNA RT-qPCRs were performed on a 7500 REAL TIME PCR SYSTEM (Applied Biosystems). mRNA real time quantification was generally performed in a two-step format using Eurogentec Reverse Transcriptase Core Kit and MESA GREEN qPCR Master Mix Plus for SYBR Assay with Low Rox kit from Eurogentec following the suppliers' protocols. Reactions were performed with 50ng of cellular RNA. The RT reaction condition was  $25^{\circ}\text{C}$ , 10 min;  $48^{\circ}\text{C}$ , 30min;  $95^{\circ}\text{C}$ , 5 min. The PCR condition was  $95^{\circ}\text{C}$ , 5 min;  $95^{\circ}\text{C}$ , 15 sec;  $60^{\circ}\text{C}$ , 1 min; for 40 cycles. The comparative  $C_t$  method which typically included normalization by 18S

rRNA levels for each sample was used for relative quantification. Details of mRNA gene specific primers are given in [Table S2](#).

Quantification of miRNA levels was done using Applied Biosystem TaqMan® chemistry based miRNA assay system. All mRNA RT-qPCRs were performed on Biorad CFX96 Real Time System. Assays were performed with 25 ng of cellular RNA, using specific primers for human miR-122, miR-16 and miR-21 (assay ID 000445, 000391, 000397 respectively, [Table S3](#)). U6 snRNA (assay ID 001973) was used as an endogenous control. One third of the reverse transcription mix was subjected to PCR amplification with TaqMan® Universal PCR Master Mix No AmpErase (Applied Biosystems) and the respective TaqMan® reagents for target miRNA. The RT reaction condition was: 16°C, 30 min; 42°C, 30 min; 85°C, 5 min; 4°C, ∞. The PCR condition was: 95°C, 5 min; 95°C, 15 sec; 60°C, 1 min; for 40 cycles. For detection of miRNAs in exosomal fractions, 100ng of RNA was used for reverse transcription.

Samples were analyzed in triplicates. The concentrations of intra cellular miRNAs and mRNAs were calculated based on their normalized  $C_t$  values. The  $\Delta\Delta C_t$  method for relative quantitation (RQ) of gene expression was used and relative quantification was done using the equation  $2^{-\Delta\Delta C_t}$  (as per 'Guide to Performing Relative Quantitation of Gene Expression Using Real-Time Quantitative PCR' obtained from the Applied Biosystems website ([http://www3.appliedbiosystems.com/cms/groups/mcb\\_support/documents/generaldocuments/cms\\_042380.pdf](http://www3.appliedbiosystems.com/cms/groups/mcb_support/documents/generaldocuments/cms_042380.pdf))).

### Identification of differentially expressed MMPs and cytokines

Differentially expressed genes (DEGs) with P value  $\leq 0.05$  were extracted from a transcriptomic dataset that compared high-fat diet fed mice with normal diet fed group (GSE163918). Up-regulated cytokines were obtained from two miR-122 KO specific GEO datasets (GSE27713 and GSE31453) with LogFC value  $\geq 1.5$ . Further, these up-regulated cytokines were mapped on to the DEGs of GSE163918. Expression status of MMPs present in the GSE163918 was also observed.

### Western blot analysis

Cells were lysed in 1X Passive Lysis Buffer (PLB) (Promega) and quantified using Bradford reagent (Thermo Scientific). Cell number equivalent amount of the sample is then diluted in 5X Sample Loading Buffer (312.5 mM Tris-HCl, pH 6.8, 10% SDS, 50% glycerol, 250 mM DTT, 0.5% bromophenol blue) and heated for 10 mins at 95°C. Usually 1/5<sup>th</sup> of the total amount from a 4cm<sup>2</sup> well was loaded for both the control and experimental samples. Following SDS-polyacrylamide gel electrophoresis of the extracts, proteins were transferred to PVDF nylon membranes. Membranes were blocked in TBS (Tris-buffered saline) containing 0.1% Tween-20 and 3% BSA. Primary antibodies were added in 3% BSA for a minimum 16 hr at 4°C. Following overnight incubation with antibody, the membranes were washed at room temperature thrice for 5 min with TBS containing 0.1% Tween-20. Washed membranes were incubated at room temperature for 1 hr with secondary antibodies conjugated with horseradish peroxidase (1:8000 dilutions). Excess antibodies were washed three times with TBS-Tween-20 at room temperature. Antigen-antibody complexes were detected with West Pico Chemi luminescent substrate using standard manufactures protocol (Perkin Elmer). Imaging of all western blots was performed using an UVP Biolumager 600 system equipped with VisionWorks Life Science software (UVP) V6.80.

### Fluorescence microscopy

Gelatin coated cover slips are added onto a 24 well plate. Recipient HeLa cells were seeded onto those cover slips such that they become 40% confluent after 24 hours. EVs from donor cells were added to 24-well inserts coated with 3mg/ml Matrigel and incubated for 24-48hrs. The recipient cells were washed with 1X PBS and fixed using 4% paraformaldehyde in 1X PBS for 30 mins in the dark at room temperature. Cover slips were then washed thrice with 1X PBS. Primary antibody incubation was done in 1XPBS with 1% BSA at 4°C overnight in a humid chamber. The anti-Tubulin antibody was used at a dilution of 1:100. Secondary antibody incubation was done in 1XPBS with 1% BSA for 1h at room temperature. Secondary anti-mouse antibodies labelled either with Alexa Fluor® 488 secondary antibodies (green) or Alexa Fluor® 568 (Red) (Invitrogen) were used at 1:500 dilutions. The cells were subsequently washed thrice with 1X PBS. Coverslips were then mounted with Vectashield containing DAPI and observed under a fluorescence microscope. Images were captured with a Zeiss LSM800 microscope. All post capture analysis and processing were done using Imaris 7 (BitPlane) software.



### **Post capture image analysis**

All western blots were processed with Adobe Photoshop CS4 for all linear adjustments and cropping. All images captured on Zeiss LSM800 microscope were analyzed and processed with Imaris 7 (Bitplane) software.

### **QUANTIFICATION AND STATISTICAL ANALYSIS**

All graphs and statistical analyses were generated in Graph-Pad Prism 5.00 (GraphPad, San Diego, CA, USA). Nonparametric unpaired t test and paired t test were used for analysis, and p values were determined. Error bars indicate mean  $\pm$  SEM.